

Dynamics of ENSO Variability and its Impact on the Indian Ocean

A Dissertation for

Course code and Course Title: MSC617 Dissertation

Credits:16

Submitted in partial fulfillment of Master's Degree

MSc in Marine Science

By

TIRTHA RAVINDRA BAGI

Roll Number: 22P0400028

ABC ID: 629961807066

PR Number: 20190311

Under the supervision of

NIKITA MANGESHKAR

School of Earth Ocean and Atmospheric Sciences

Marine Sciences



Goa University

April 2024



Examined by:

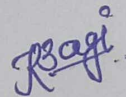
Seal of the School

DECLARATION BY STUDENT

I hereby declare that the data presented in this Dissertation report entitled “Dynamics of ENSO Variability and its Impact on the Indian Ocean” is based on the results of investigations carried out by me in the Discipline of Marine Sciences at the School of Earth, Ocean and Atmospheric Sciences, Goa University under the Supervision of Ms. Nikita Mangeshkar and the same has not been submitted elsewhere for the award of a degree or diploma by me. Further, I understand that Goa University or its authorities will not be responsible for the correctness of observations/experiments or other findings given in the dissertation.

I hereby authorize the University authorities to upload this dissertation to the dissertation repository or anywhere else as the UGC regulations demand and make it available to anyone as needed.

Date: 30/4/24
Place: Goa University, Taleigão Plateau, Goa



Tirtha Ravindra Bagi
Seat No: 22P0400028

COMPLETION CERTIFICATE

This is to certify that the dissertation report “**Dynamics of ENSO Variability and its Impact on the Indian Ocean**” is a bonafide work carried out by **Ms. Tirtha Ravindra Bagi** under my supervision in partial fulfillment of the requirements for the award of the degree of **Master of Science** in the Discipline of Marine Sciences at the School of Earth, Ocean and Atmospheric Sciences, Goa University.

Date: 30/04/2024

Ms. Nikita Mangeshkar
Discipline of Marine Sciences,
School of Earth, Ocean and Atmospheric Sciences

Sr. Prof. Sanjeev C. Ghadi,
Senior Professor and Dean
Marine Sciences
School of Earth, Ocean and Atmospheric Sciences

Date:

Place: Goa University, Taleigão Plateau, Goa



School Stamp

CONTENTS

Chapter	Contents	Page Numbers
	Preface	I-II
	Acknowledgment	III
	List of Abbreviations	IV
	List of Figures	V-VI
	List of Tables	VII
	Abstract	VIII
1.	Introduction	1-7
	1.1 Background	1-5
	1.1.1 El-Nino Phase	
	1.1.2 La-Nina Phase	
	1.1.3 Neutral Phase	
	1.2 Aim and Objective	6
	1.3 Scope	6
2.	Literature Review	8-14
3.	Data and Methodology	15-17
	3.1 Sea Surface Temperature	
	3.2 Sea Surface Temperature Anomaly (SSTA)	
	3.3 Oceanic Nino Index (ONI)	
	3.4 Precipitation over the Indian Ocean	
4.	Analysis and Conclusion	18-59
	4.1 Sea Surface Temperature	
	4.2 Sea Surface Anomaly	
	4.3 Oceanic Nino Index	
	4.4 Precipitation Over Indian Ocean	

4.5 Discussion

4.5.1 Sea Surface Temperature

4.5.2 Sea Surface Temperature Anomaly

4.5.3 Oceanic Nino Index

4.5.4 Precipitation Over Indian Ocean

4.6 Conclusion

References

60-62

PREFACE

The El Niño-Southern Oscillation (ENSO) phenomenon is a crucial driver of global climate variability, characterized by fluctuations in sea surface temperatures (SST) across the tropical Pacific Ocean. The study of ENSO is essential for comprehending the intricate dynamics of weather patterns, marine ecosystems, and extreme events worldwide.

ENSO manifests in three primary phases: El Niño, La Niña, and neutral. El Niño events are marked by warmer-than-average SST in the central and eastern tropical Pacific, disrupting atmospheric circulation patterns. During El Niño, weakened trade winds and reduced upwelling of cold water alter weather conditions globally, leading to droughts, floods, and temperature anomalies. The impacts of El Niño are far-reaching, affecting agriculture, water resources, and vulnerable communities across continents. Marine ecosystems experience ecological shifts during El Niño, with changes in nutrient availability and species distribution impacting fisheries and biodiversity.

Conversely, La Niña events are characterized by cooler-than-average SST in the central and eastern tropical Pacific, intensifying atmospheric circulation patterns. Stronger trade winds and enhanced upwelling during La Niña influence weather patterns differently, leading to increased precipitation in some regions and droughts in others. La Niña events have significant implications for agriculture, water management, and disaster risk reduction efforts. Marine ecosystems also respond to La Niña, with changes in nutrient dynamics and species distribution affecting fisheries and ecosystems.

Neutral phases of ENSO occur when SSTs are close to average, but atmospheric conditions may exhibit El Niño or La Niña-like characteristics. These periods are crucial for understanding the transition between ENSO phases and their impacts on climate variability. Neutral phases provide opportunities for studying the underlying mechanisms driving ENSO and refining climate prediction models.

The influence of ENSO extends beyond atmospheric dynamics to marine ecosystems, where temperature anomalies affect nutrient availability, primary productivity, and species distribution. ENSO-driven fluctuations in ocean conditions impact fisheries, coral reefs, and marine biodiversity, highlighting the interconnectedness of oceanic and atmospheric processes.

In addition to its influence on weather and marine ecosystems, ENSO plays a pivotal role in shaping the frequency and intensity of extreme weather events globally. El Niño and La Niña events can exacerbate or mitigate the occurrence of hurricanes, typhoons, droughts, and floods, posing significant risks to human populations and ecosystems. Understanding ENSO's influence on extreme events is critical for enhancing disaster preparedness, early warning systems, and resilience-building efforts.

Overall, unraveling the complexities of ENSO is essential for understanding global climate variability and mitigating its impacts on weather patterns, marine ecosystems, and extreme events. By integrating ENSO information into climate modeling, forecasting, and adaptation strategies, we can enhance resilience and adaptability to climate-related challenges and safeguard vulnerable communities and ecosystems against the impacts of ENSO-driven variability.

ACKNOWLEDGEMENTS

I would like to express my heartfelt gratitude to God for granting me strength throughout the journey of completing this dissertation. I extend my deepest appreciation to my family for their support.

A special word of thanks goes to my guide Ms. Nikita Mangeshkar, Assistant Professor, at the School of Earth, Ocean and Atmospheric Sciences, Goa University, for her invaluable support and guidance throughout the dissertation process. Her expertise, patience, and encouragement have been instrumental in shaping this work and navigating through its complexities.

I would like to thank Sr. Prof. Sanjeev C. Ghadi, Dean of the School of Earth, Ocean and Atmospheric Sciences, Goa University, and Sr. Prof. C. U. Rivonker, Former Dean of School of Earth, Ocean and Atmospheric Sciences, for providing the necessary facilities that aided in the completion of my dissertation work.

Additionally, I would like to thank the data providers –The data is of Sea Surface Temperature from the website neo.gsfc.nasa.gov. The data was downloaded from the web pages: neo.gsfc.nasa.gov. The Data for precipitation was downloaded from the ERA5 website. The data was downloaded from the webpage: cds.climate.copernicus.

I would also like to extend my heartfelt appreciation to my dear friend Miss. Ashis Karthika, Krutika Devashetti, and Satwik Bagi for their assistance and support. Their willingness to lend a helping hand, and offer insightful advice, is deeply appreciated. In this journey, I offer my sincere gratitude to everyone who has played a part, no matter how big or small.

LIST OF ABBREVIATIONS

Entity	Abbreviation
Sea Surface Temperature	SST
Sea Surface Temperature Anomaly	SSTA
Oceanic Nino Index	ONI
Milli Meter	mm
Degree Celsius	⁰ C

LIST OF FIGURES

Figure Number	Description	Page Number
4.1.1	Monthly Mean of Sea Surface Temperature Over A Super Strong La-Nina Year 2010-2011.	18-19
4.1.2	Monthly Mean of Sea Surface Temperature Over A Super Strong El-Nino Year 2015-2016.	21-22
4.1.3	Monthly Mean Of Sea Surface Temperature Over A Strong El-Nino Year 2023.	24
4.2.1	Sea Surface Temperature Anomaly over the Nino 3.4 region during August 2012.	26
4.2.2	Sea Surface Temperature Anomaly over the Nino 3.4 region during Weak LaNina phase observed from August 2005 to February 2006.	27
4.2.3	Sea Surface Temperature Anomaly over the Nino 3.4 region during supper strong LaNina phase observed from June 2010 to May 2011.	29-30
4.2.4	Sea Surface Temperature Anomaly over the Nino 3.4 region during weak El-Nino phase observed from April 2006 to March 2007.	32-33
4.2.5	Sea Surface Temperature Anomaly over the Nino 3.4 region during the super strong El-Nino phase observed from April 2015 to March 2016.	34-35
4.4.1	Precipitation over the Indian Ocean in the year 2010 (strong La-Nina year).	44
4.4.2	Precipitation over the Indian Ocean in the year 2015 a super strong El-Nino year.	46
4.5.1	Monthly Mean Of Sea Surface Temperature over a) August 2012 b) August 2010 c) August 2015 d) September 2012 e)September 2012 f) October 2012.	49
4.5.2	Variation of SSTA over 40 years over the Nino 3.4 region.	51

4.5.3	Variation of ONI over last 40 years over the Nino 3.4 region.	53
4.5.4	Total precipitation over the Indian Ocean region from June to August 2010 and 2015.	55

LIST OF TABLES

Table number	Description	Page number
4.3.1	Table showing the monthly variation of the Oceanic Nino Index.	37
4.5.1	El-Nino phases observed over the last 40 years	54
4.5.2	La-Nina Phases observed over the last 40 years.	54

ABSTRACT

This study utilizes NOAA and ERA5 monthly averaged data to analyze the Sea Surface Temperature and precipitation of the year from 1982 to 2023, employing Python programming to generate contour plots. Subsequently, the same dataset is examined over the Indian Ocean for the years 2010 and 2015, highlighting the yearly fluctuations over the Sea Surface Anomaly and the Oceanic Nino Index. The Sea Surface Temperature plots are constructed to understand the ENSO phenomena and the precipitation plots are constructed to understand the impact of ENSO over the Indian Ocean.

CHAPTER 1: INTRODUCTION

1.1 Background

The sun, as the primary energy source, heats the Earth's surface, particularly over the Pacific Ocean, leading to the evaporation of water. When this evaporated water condenses into rain, it releases significant heat, creating dynamic atmospheric circulation patterns. These processes, centered around the equator, are referred to as equatorial phenomena. Equatorial currents play a crucial role in shaping air-sea interactions, notably influencing phenomena like El Niño-Southern Oscillation, which has far-reaching global effects (**Stewart et al., 1992**). According to **Philander et al. (1999)**, the sailors in Peru were the first to observe this phenomenon. As they navigated along the coast, they encountered a current that ran contrary to their expectations, either to the north or to the south of the port. They named this counter-current "El Niño," meaning "the Jesus child," as it was often observed shortly after Christmas.

The El Niño-Southern Oscillation (ENSO) is a recurring climate pattern involving changes in the temperature of waters in the central and eastern tropical Pacific Ocean for periods ranging from about three to seven years, the surface waters across a large swath of the tropical Pacific Ocean warm or cool by anywhere from 1°C to 3°C, compared to normal. This oscillating warming and cooling pattern, referred to as the ENSO cycle, directly affects rainfall distribution and chlorophyll in the tropics and can have a strong influence on weather across the United States and other parts of the world. El Niño and La Niña are the extreme phases of the ENSO cycle; between these two phases is a third phase called ENSO-neutral (<http://www.bom.gov.au/climate/about/australian-climate-influences.shtml?bookmark=enso>).

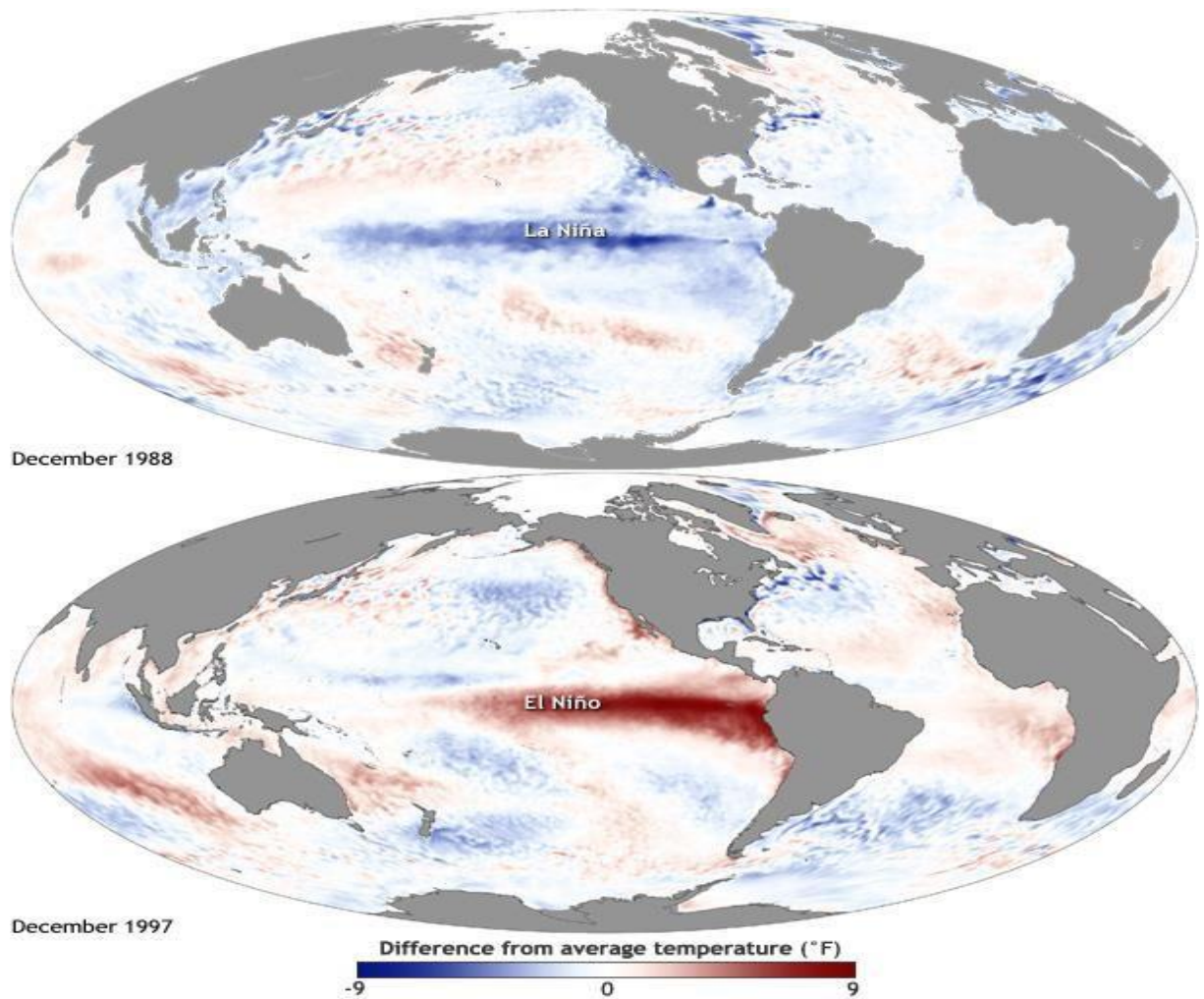


Fig 1.1 Phases of ENSO (La-Niña and El-Niño)

Image source: <https://www.climate.gov/news-features/understanding-climate/el-ni%C3%B1o-and-la-ni%C3%B1a-frequently-asked-questions>

1.1.1 El-Niño phase

El Niño is a climatic phenomenon characterized by warmer-than-average sea surface temperatures in the central and eastern tropical Pacific Ocean. This warming alters global weather patterns, reducing rainfall in Indonesia and increasing precipitation in the central and eastern Pacific regions. Typically, the easterly trade winds along the equator weaken or reverse direction during El Niño events (<http://www.bom.gov.au/climate/about/australian-climate>). This phenomenon disrupts normal oceanic processes, such as upwelling, where cold, nutrient-rich water rises from the depths. During El Niño, upwelling weakens or ceases, resulting in decreased nutrient availability and reduced phytoplankton populations along the Pacific coast. This disruption cascades through the marine food web, impacting fish

populations and the entire ecosystem. Additionally, the warmer waters associated with El Niño can attract tropical species to normally colder areas (Noaa climate.gov).

The atmospheric circulation patterns during El Niño events, known as the Walker Circulation, shift eastward, with rising air over the anomalously warm central and eastern Pacific Ocean and sinking air over the Maritime continent and northern South America. These changes in atmospheric circulation further contribute to the altered weather patterns associated with El Niño (Noaa climate.gov).

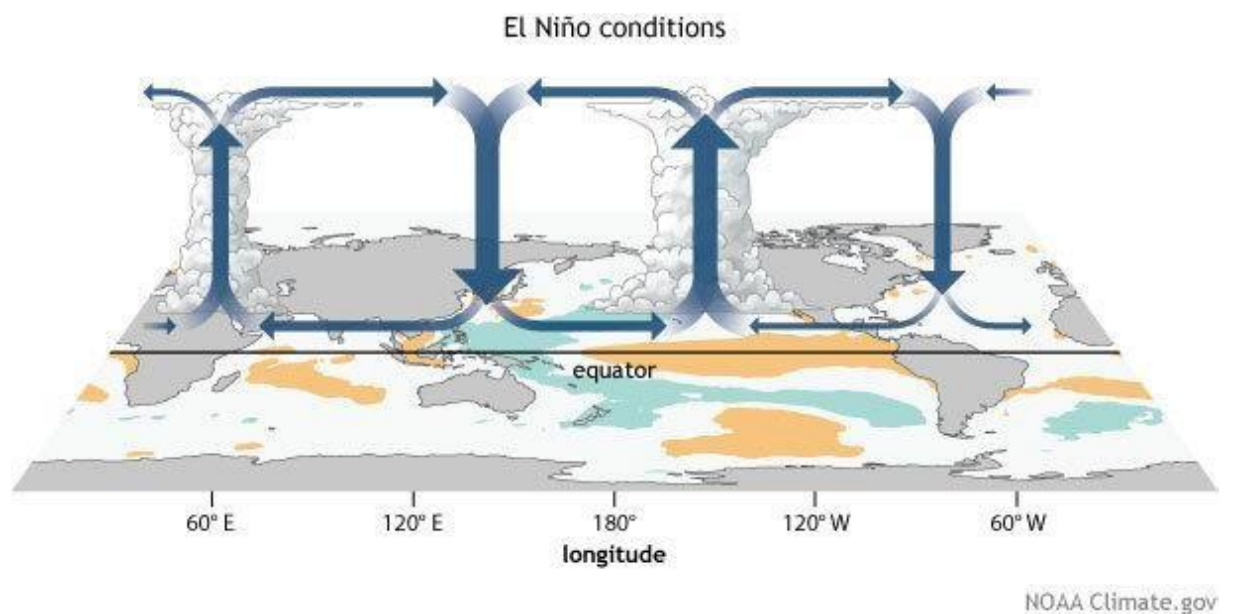


Fig 1.2 Walker circulation shifting eastward during El Niño.

Image source: <https://www.climate.gov/news-features/understanding-climate/el-ni%C3%B1o-and-la-ni%C3%B1a-frequently-asked-questions>

1.1.2 La-Niña Phase

La Niña is a climatic phenomenon marked by cooler-than-average sea surface temperatures in the central and eastern tropical Pacific Ocean. This cooling alters global weather patterns, resulting in increased rainfall in Indonesia and decreased precipitation in the central and eastern Pacific regions. Typically, the easterly trade winds along the equator become even stronger during La Niña events (<http://www.bom.gov.au/climate/about/australian-climate-influences.shtml?bookmark=enso>).

The atmospheric circulation patterns during La Niña events, akin to the Walker Circulation, shift towards the west with rising air over the cooler central and eastern Pacific Ocean and

sinking air over the Maritime continent and northern South America. These alterations in atmospheric circulation further influence the distinct weather patterns associated with La Niña.

This phenomenon affects oceanic processes such as upwelling, where cold, nutrient-rich water ascends from the depths. During La Niña, upwelling intensifies, leading to increased nutrient availability and enhanced phytoplankton populations along the Pacific coast. This influence propagates through the marine food web, impacting fish populations and the overall ecosystem. Additionally, the cooler waters linked with La Niña can deter tropical species from their typical habitats (Noaa climate.gov).

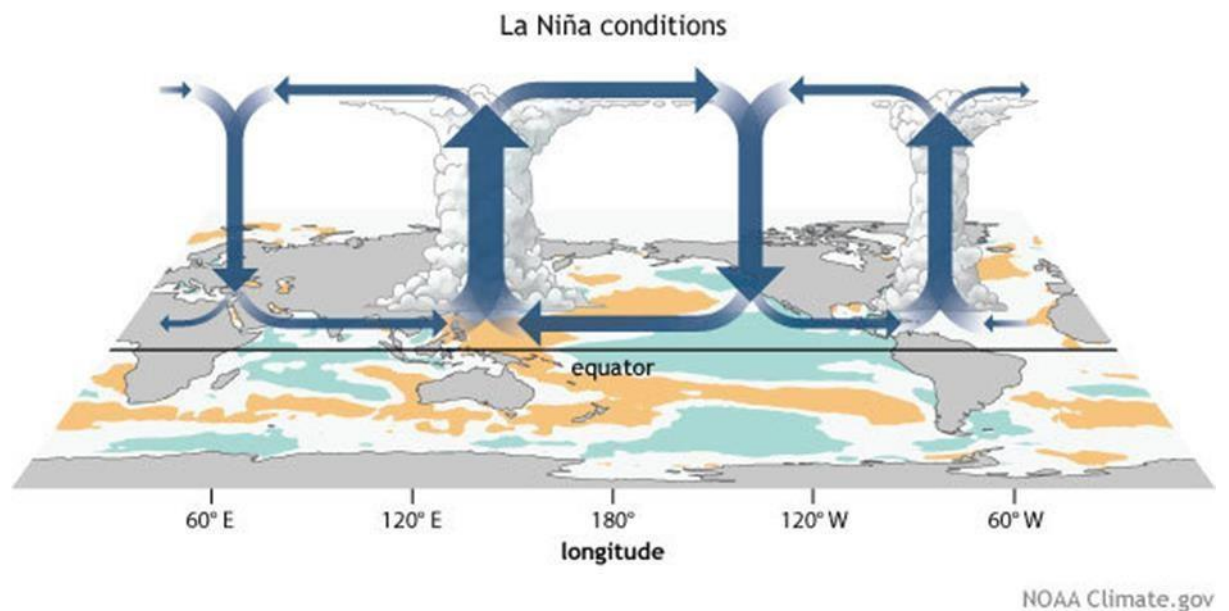


Fig 1.3 Walker circulation during La-Nina shifting west words

Image source: <https://www.climate.gov/news-features/understanding-climate/el-ni%C3%B1o-and-la-ni%C3%B1a-frequently-asked-questions>

1.1.3 Neutral Phase

Neither El Niño or La Niña occur during this phase. Often tropical Pacific SSTs are generally close to average. However, there are some instances when the ocean can look like it is in an El Niño or La Niña state, but the atmosphere is not playing along or vice versa (<http://www.bom.gov.au/climate/about/australian-climateinfluences.shtml?bookmark=enso>).

Generalized Walker Circulation (December-February) during ENSO-neutral conditions. Convection associated with rising branches of the Walker Circulation is found over the Maritime continent, northern South America, and eastern Africa (Noaa climate.gov).

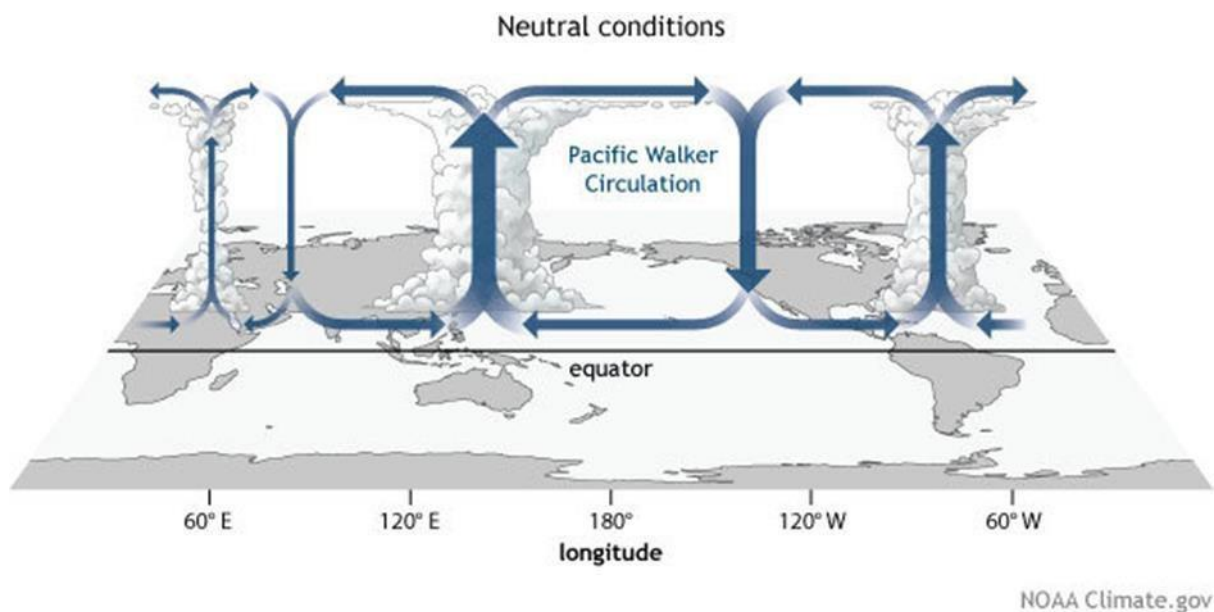


Fig 1.4 Walker circulation during the neutral phase

Image source: <https://www.climate.gov/news-features/understanding-climate/el-ni%C3%B1o-and-la-ni%C3%B1a-frequently-asked-questions>

1.2 Aim and Objective

- Understanding ENSO over the last 40 years.
- Studying the impact of ENSO on the Indian Ocean.
- Assessing the impact of ENSO for the next few years using preexisting data.

1.3 Scope

Understanding the processes behind El Niño-Southern Oscillation (ENSO) events is crucial for grasping the intricate dynamics of global climate variability. ENSO stands as one of the most influential drivers of climate variability worldwide. By delving into the mechanisms that propel ENSO occurrences, we gain invaluable insights into how these phenomena ripple across the globe, shaping weather patterns, temperature anomalies, and precipitation distributions in diverse regions.

This understanding serves as the bedrock for advancing climate modeling and forecasting capabilities. By deciphering how ENSO events evolve and impact atmospheric circulation patterns, we can refine weather forecast accuracy, especially for forecasting seasons and long-range outlooks. Integrating ENSO information into forecast models empowers us to anticipate potential temperature extremes, droughts, floods, and other weather-related hazards more effectively.

The impact of ENSO transcends atmospheric dynamics, extending its influence to marine ecosystems. ENSO-driven fluctuations in ocean surface temperatures, characterized by El Niño and La Niña events, wield significant consequences for marine habitats and species. These temperature shifts disrupt ecosystems, alter nutrient availability, and profoundly influence the distribution and abundance of marine life. Understanding these dynamics is indispensable for guiding fisheries management, conservation efforts, and evaluating ecosystem resilience in the face of climate variability.

Moreover, ENSO plays a pivotal role in shaping the frequency and intensity of extreme weather events globally. Whether exacerbating or mitigating the occurrence of hurricanes, typhoons, droughts, or other extreme events, ENSO's influence on atmospheric and oceanic

processes cannot be understated. Armed with insights into these mechanisms, we can proactively assess and manage risks associated with extreme weather events. This includes implementing early warning systems, devising adaptation strategies, and bolstering disaster risk management measures to mitigate the impacts of ENSO-related extremes on vulnerable populations and ecosystems.

In essence, comprehending the complexities of ENSO is fundamental not only for revealing the intricacies of global climate variability but also for safeguarding against its far-reaching impacts on weather, marine ecosystems, and extreme weather events.

CHAPTER 2: LITERATURE REVIEW

(**Cane et al., 2005**) The study examined irregular oscillations of the El Niño Southern Oscillation (ENSO) cycle that occur approximately every 2-7 years. Bjerknes' feedback mechanism, coupled with wave propagation dynamics, forms the "delayed oscillator" system, where warming (El Niño) and cooling (La Niña) phases alternate. The oscillation period is determined by the balance between direct and delayed signals influenced by coupling strength. While linear models offer insights, nonlinear complexities maintain periods within the 2-7-year range. The irregularity of ENSO cycles is attributed to chaotic dynamics and noise from weather systems, complicating predictions and understanding.

(**Tudhope et al., 2001**) The study utilizes annually-banded coral records from Papua New Guinea to investigate the variability of the El Niño–Southern Oscillation (ENSO) over the past 130,000 years. It reveals that ENSO has persisted throughout glacial and interglacial periods, with the 20th century experiencing notably strong ENSO events compared to previous epochs. The observed changes in ENSO strength are attributed to a combination of dampening effects during glacial conditions and forcing by precessional orbital variations. This dual control mechanism sheds light on the sensitivity of ENSO to global climate changes, crucial for predicting its future behavior under greenhouse warming.

(**Harrison et al., 1998**) The study examines ENSO periods post-World War II, analysing sea surface temperature and wind anomalies using COADS data. It identifies common patterns across ENSO phases and introduces the Bjerknes ENSO Index (BEI) to classify event magnitudes. Findings challenge traditional ENSO notions, highlighting the role of meridional winds and questioning trade wind dynamics. The study notes anomalous patterns in the tropical Indian Ocean and extratropical regions. Despite data limitations, it underscores the importance of understanding ENSO dynamics for climate prediction. Written in October 1997, it references TOGA observations and COADS data, likely spanning the post-WWII period up to the late 1990s.

(McPhaden et al., 2006) The study highlights ENSO events are associated with a weakening of trade winds in the equatorial Pacific and lead to warming in the central and eastern Pacific and cooling in the western Pacific. Though it originates in the Pacific, it affects the global weather pattern.

(Wang et al.,2023) The study explores the application of deep learning (DL) techniques to predict El Niño/Southern Oscillation (ENSO) events, crucial for understanding global climate patterns. Utilizing diverse datasets including sea surface temperature (SST) and atmospheric variables, various DL models like recurrent neural networks (RNNs) and convolutional neural networks (CNNs) were employed. Evaluation metrics such as correlation coefficient and root mean square error were utilized to assess model performance. Techniques to overcome the spring predictability barrier (SPB) and address prediction uncertainty were investigated. The study showcases promising results, indicating DL's potential in enhancing ENSO prediction accuracy and warrants further exploration in overcoming data limitations and improving model robustness.

(Ren et al., 2019) The study focused on analysing seasonal variations in Sea Surface Temperature (SST) and chlorophyll-a concentration in the South China Sea (SCS) region, employing a range of datasets. These included MODIS satellite images for chlorophyll-a and SST data, obtained from 2003 to 2017 with a resolution of 4 km. Additionally, CCMP wind data were utilized to understand wind patterns and their impact on SST and chlorophyll-a distribution, calibrated to produce high-resolution analysis grids. The Oceanic Niño 3.4 Index (ONI 3.4) from NOAA served to identify the influence of El Niño-Southern Oscillation (ENSO) on SST and chlorophyll-a, discerning periods of El Niño, La Niña, and normal conditions. Results unveiled distinct seasonal patterns influenced by monsoon winds, affecting temperature and nutrient distribution. ENSO emerged as a significant factor, with El Niño events correlating with increased SST and reduced chlorophyll-a concentration, and La Niña events exhibiting the reverse. Correlation analyses underscored strong positive links between ENSO and SST, particularly in the western SCS, but revealed

a more nuanced relationship between ENSO and chlorophyll-a, indicating additional influences such as wind patterns and nutrient supply. The study underscored the importance of integrating meteorological and oceanographic factors for a comprehensive understanding of SST and chlorophyll-a dynamics in the SCS, particularly in light of ENSO variability.

(Choi et al., 2023) A study focused on predicting Korean Peninsula SSTs to mitigate fish farm damage from global warming. Using ECMWF ERA5 data, LSTM models trained with 12-20 years data were more accurate than 5 years. Validation with NOAA OI SST v2 showed similar performance. Future work involves pixel-level optimization for better predictions, aiding early high-water temperature warnings.

(Bader et al., 2003) The study utilized observational data from 1951 to 1994 and employed the ECHAM4.5 atmospheric model forced by observed sea surface temperatures (SSTs) to investigate Sahelian rainfall trends. It identified a significant multidecadal drying trend in the Sahel from the 1950s to the 1990s, associated with variations in tropical SST anomalies, particularly in the Indian Ocean. Results showed that anomalously cold tropical Indian Ocean SSTs contributed to reduced Sahelian rainfall, indicating the pivotal role of Indian Ocean SSTs in driving decadal climate variability, influencing both regional and extratropical climate patterns.

(Glantz et al., 2020) The study collected historical data on sea surface temperatures (SSTs) in the central Pacific Ocean to monitor El Niño episodes. Specifically, they focused on the Oceanic Niño Index (ONI), which records the occurrence and duration of El Niño events based on SST monitoring. They proposed that an ONI value of 0.7°C could serve as a tipping point indicating the locked-in phase of an El Niño event, providing additional lead time for societal decision-makers to take mitigative actions.

(Yehia et al., 2016) The study utilized monthly datasets of mean surface air temperature and precipitation rate for the Kingdom of Saudi Arabia (KSA) from 1950 to 2015. Additionally, El Niño 3.4 monthly data and the Oceanic Niño Index (ONI) were employed. Analysis techniques included time series, anomaly, and correlation coefficient methods.

Results indicated that KSA's climate parameters, particularly temperature and precipitation rates, were primarily influenced by ONI during the autumn and winter seasons.

(Trenberth et al., 2002) The study discusses the historical evolution and various definitions of El Niño, emphasizing the need for precise definitions to avoid confusion. It explores different quantitative criteria for identifying El Niño events, focusing on sea surface temperature (SST) anomalies in specific regions such as Niño 3 and Niño 3.4. By analysing SST data from 1950 to 1998, the study identifies El Niño and La Niña events based on thresholds and durations of SST anomalies, showing a distribution of events throughout the years. The research highlights the seasonality of ENSO events, indicating a preference for onset and transition times between March and September, despite peak amplitudes occurring in northern winters.

(Wolter et al., 2005) The Multivariate ENSO Index MEI and MEI.ext provide a comprehensive approach to monitoring ENSO activity, capturing its multivariate nature and offering greater reliability than single-variable indices. They account for seasonal variations and spatial changes, extending analysis back to 1871 and revealing historical patterns of ENSO behavior. Despite correlations with other indices, the MEI and MEI.ext offer distinct advantages in understanding ENSO variability and its implications for climate research and prediction.

(Emile-Geay et al., 2007) The study investigates the impact of solar and orbital forcing on Earth's climate dynamics, focusing on the El Niño-Southern Oscillation (ENSO) phenomenon. By analysing model simulations and paleoclimate data, the researchers find that solar and orbital forcing can induce ENSO-like variability on centennial-to-millennial timescales. This finding suggests that changes in solar irradiance and Earth's orbital parameters may have influenced ENSO activity throughout the Holocene. The study further proposes a mechanism whereby solar forcing affects tropical Pacific SSTs, subsequently influencing atmospheric circulation patterns and climate variability in regions such as North America, the North Atlantic, and the Asian monsoon. These findings provide insights into

the complex interactions between solar forcing, orbital parameters, and ENSO dynamics, highlighting the role of ENSO as a mediator of solar influence on global climate.

(Liyanage et al., 2022) This research in Kalutara, Sri Lanka, highlights the intricate relationship between climate factors (rainfall, temperature, and the Oceanic Niño Index - ONI), *Aedes* mosquito activity, and dengue risk. It reveals that rainfall above 200 mm/month significantly impacts mosquito breeding, while temperatures above 31.5°C increase vector indices after 1-2 months. El Niño events, linked to higher temperatures and altered rainfall patterns, elevate vector indices about 6 months later. These findings underscore the complex interplay of climate, vector dynamics, and disease transmission, aiding in targeted dengue prevention strategies.

(Belliard et al., 2021) The study analysed tidal gauge records from 1984 to 2017 across the Guayas Delta–Gulf of Guayaquil, Ecuador. Quality-controlled data revealed complex interactions between oceanic and meteorological forces, particularly during El Niño events. While downstream and upstream regions showed strong relationships between sea level anomalies (SLAs) and El Niño proxies, midstream regions exhibited weaker correlations. This suggests a nuanced interplay of factors, including local dynamics like bathymetry and mangrove elevation, influencing SLAs, and complicating predictive models. Non-EP-El Niño events displayed varied responses, influenced by factors such as Pacific SSTAs, Walker circulation, and extratropical teleconnections.

(Builes-Jaramillo et al., 2023) The study examined the impact of abrupt transitions between El Niño and La Niña phases on climatic patterns over northern South America. Results show significant anomalies in sea surface temperatures, precipitation, wind speeds, and water vapor transport during these transitions. Notably, the transitions induce changes in the Walker circulation, leading to alterations in precipitation patterns and low-level jet dynamics. These findings contribute to understanding the regional hydroclimatic processes influenced by ENSO transitions, highlighting their relevance for climatic diagnostics and water resource management. However, the study acknowledges limitations in sample size

and classification methodology, necessitating further research on ENSO transitions' interaction with other climatic phenomena and their implications for climate change.

(Zhou et al., 2023) The study shows how different decaying phases of El Niño (Rapid Decay - RD, and Slow Decay - SD) influence Western North Pacific (WNP) tropical cyclone (TC) activity. RD El Niño leads to a weakened monsoon trough, suppressed TC genesis, and a strengthened western Pacific subtropical high. In contrast, SD El Niño maintains a stronger monsoon trough and allows for more TC formation. These differences are attributed to variations in atmospheric circulation anomalies, particularly the anomalous Walker circulation and large-scale divergent motion. RD El Niño induces a dipole pattern across the tropical Indo-Pacific Ocean, enhancing upper-level convergence over the WNP and suppressing TC frequency. In contrast, SD El Niño exhibits a tripole pattern with less pronounced effects on WNP TC activity. Overall, the study suggests that distinct SST evolution, particularly over the tropical Indian Ocean, influences the connection between different El Niño decay phases and WNP TC activity.

(Zhang et al., 2022) The study conducted by Zhang et al looks at droughts in Yunnan Province over 58 years, paying close attention to where and when they happen. It finds that droughts have been getting worse over time, mostly occurring from January to May and hitting the eastern and southern parts of Yunnan the hardest. Using a method called SAD, the researchers pinpoint six big drought events, which match what other studies have found. They also link droughts to El Niño and La Niña weather patterns, showing that these can lead to dry spells at different times of the year. Despite using limited data, the study suggests that future research should consider more factors, like humidity, temperature, and human activities, to understand better and prepare for droughts in Yunnan.

(Derot et al., 2024) The study done by, researchers examined whether applying the signature method could enhance climate forecasting models. They compared different models to gauge their effectiveness in predicting climate phenomena such as El Niño and La Niña. Results showed that while the signature method improved the performance of models like

Lasso and LSTM, it had minimal impact on others like Random Forest (RF). Additionally, the analysis revealed significant interactions between various climate factors, such as sea surface temperatures and atmospheric pressure, influencing the occurrence of El Niño and La Niña events. These findings suggest that the signature method could offer valuable insights for better understanding and forecasting future climate changes.

(Wang et al., 2021) The study evaluated a novel approach for predicting El Niño events up to a year in advance, showing promising results. The proposed method effectively forecasted El Niño-related temperatures for 2008–2019, with low errors. It accurately identified El Niño years and captured their trends. Compared to other models, it demonstrated superior performance, even outperforming recent machine learning methods. Additionally, it surpassed classical machine learning algorithms like Support Vector Regression and K-Nearest Neighbours, providing more reliable long-term forecasts. However, challenges remain in accurately predicting very strong El Niño events. Overall, the study confirms the effectiveness of the proposed approach in predicting El Niño events with a 12-month lead time, suggesting its potential for practical applications in climate forecasting.

CHAPTER 3: DATA AND METHODOLOGY

3.1 Sea Surface Temperature

For plotting the sea surface temperature map over the global region satellite observations from instruments like the Advanced Very High-Resolution Radiometer (AVHRR) were utilized to capture thermal radiation emitted by the sea surface. The data spanned from 1982 to 2023 and were obtained at a spatial resolution of $1^\circ \times 1^\circ$. These data were accessed as a CSV file from the NASA website https://neo.gsfc.nasa.gov/view.php?datasetId=AVHRR_SST_M and [Sea Surface Temperature \(1 month - Aqua/MODIS\) | NASA](#), specifically the Sea Surface Temperature (SST) dataset under the Aqua/MODIS mission. The global map of SST is plotted using Python programming. Pandas, Numpy, Matplotlib, and Cartopy are the modules of python programming that were used to plot the maps.

3.2 Sea Surface Temperature Anomaly (SSTA)

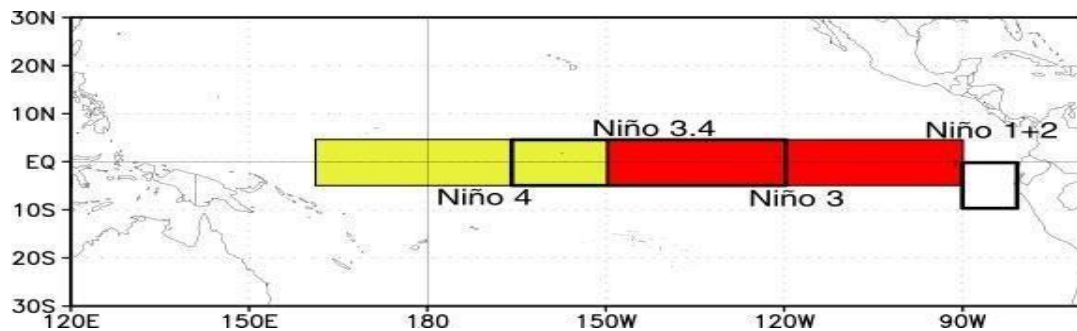


Fig 3.1 shows the various regions used to calculate ONI that is the Nino1, Nino 2, Nino 3, Nino 4 and 3.4

Image source: https://www.researchgate.net/figure/Map-of-Map-of-geographic-regions-of-Nino-1-2-3-and-34-sea-surface-temperature-SST_fig1_255681593

To plot the sea surface temperature anomaly over the Nino 3.4 region satellite observations from instruments like the Advanced Very High-Resolution Radiometer (AVHRR) were utilized to capture thermal radiation emitted by the sea surface. The data spanned from 1982 to 2023 and were obtained at a spatial resolution of $1^\circ \times 1^\circ$. These data were accessed as a CSV file from the NASA website, specifically the Sea Surface Temperature (SST) dataset under the Aqua/MODIS mission. The Nino

3.4 region Monthly mean SST values are calculated for this region, followed by the calculation of 30-year mean. The SST values are calculated by subtracting the 30-year mean value from the monthly mean values. Niño-1, Niño-2, Niño-3, and Niño-4 regions are geographical areas in the tropical Pacific Ocean where sea surface temperature anomalies are monitored to gauge ENSO conditions. Each region plays a distinct role in understanding ENSO's strength and spatial distribution. The Niño 3.4 region is a segment of the equatorial Pacific Ocean spanning from approximately 120°W to 170°W longitude and 5°N to 5°S latitude. Niño-3.4, located in the central Pacific, The Niño 3.4 region serves as a key indicator for monitoring and predicting El Niño and La Niña events, which can have profound impacts on global weather patterns. By analyzing sea surface temperature anomalies in this region scientists can anticipate shifts in weather phenomena such as droughts, floods, and hurricanes, allowing for better preparation and mitigation efforts (https://www.researchgate.net/figure/Map-of-Map-of-geographic-regions-of-Nino-1-2-3-and-34-sea-surface-temperature-SST_fig1_255681593).

The map is plotted using a Python program. Pandas, Numpy, Matplotlib, and Cartopy are the modules of Python programming that were used to plot the maps.

3.3 Oceanic Nino Index (ONI)

To calculate the Oceanic Nino Index the seasonal averages through the year are calculated over the Nino 3.4 region. The climatic mean of the temperature is taken for the period (1982-2023). However, the interactive plotting and analysis are done by using Microsoft Excel and Python programming. The Oceanic Niño Index (ONI) is a key tool NOAA uses to classify El-Niño and La-Niña events in the eastern tropical Pacific. It calculates the running 3-month mean sea surface temperature (SST) anomaly in the Niño 3.4 region. El Niño events are defined by 5 consecutive periods with SST anomalies of +0.5°C or higher, while La Niña events require anomalies of -0.5°C or lower. These events are further categorized as Weak (0.5 to 0.9°C), Moderate (1.0 to 1.4°C), Strong (1.5 to 1.9°C), or Very Strong ($\geq 2.0^\circ\text{C}$) based on the extent and duration of the anomaly. This classification system ensures a standardized approach to understanding and predicting these significant climate phenomena (<https://ggweather.com/enso/oni.htm>).

3.4 Precipitation over the Indian Ocean

ERA5, the ECMWF's fifth-generation reanalysis, offers global climate data since 1940, blending models and observations. It provides spatial data of $0.25^\circ \times 0.25^\circ$ grid for hourly and monthly estimates of various atmospheric, oceanic, and land-surface variables. Monthly data, available in GRIB format, is updated with a 5-day latency, aiding diverse climate applications with its comprehensive and regularly updated datasets. The data is downloaded as a NetCDF (.nc) file and used to plot maps that showcase precipitation over the Indian Ocean (40°N , -60°S , 140°E , and 0°W).

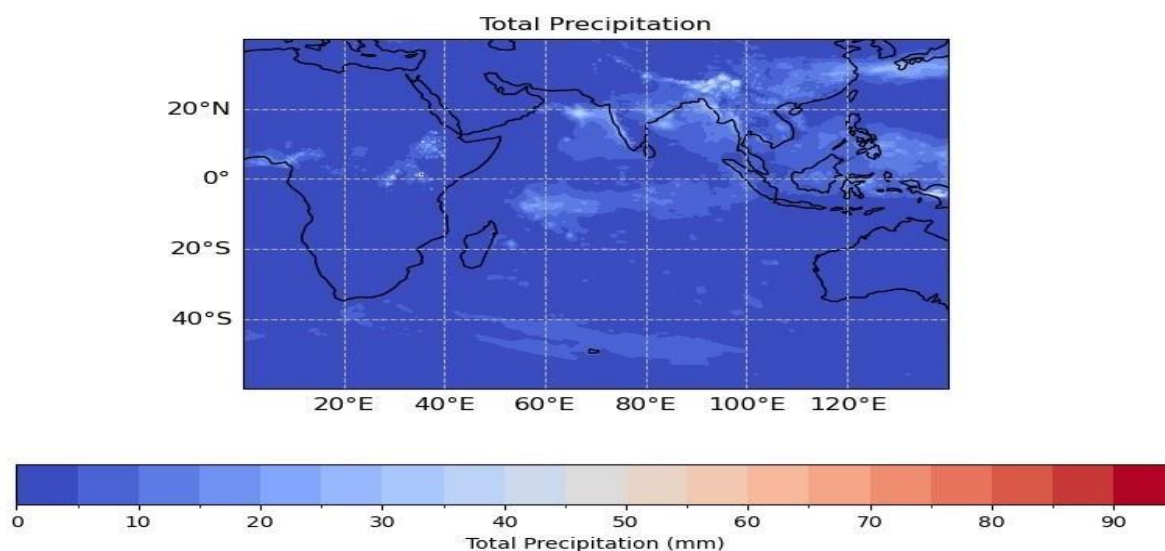
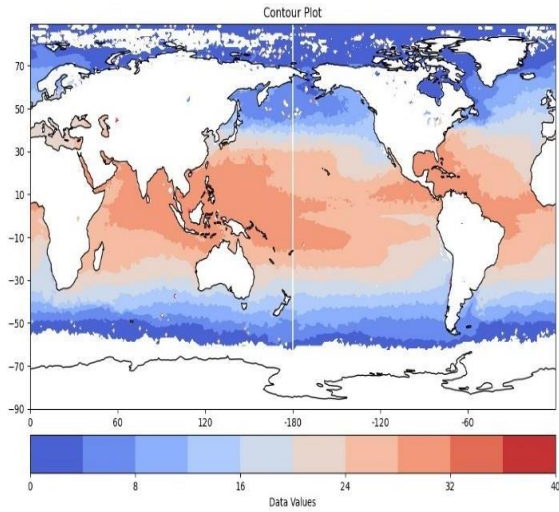


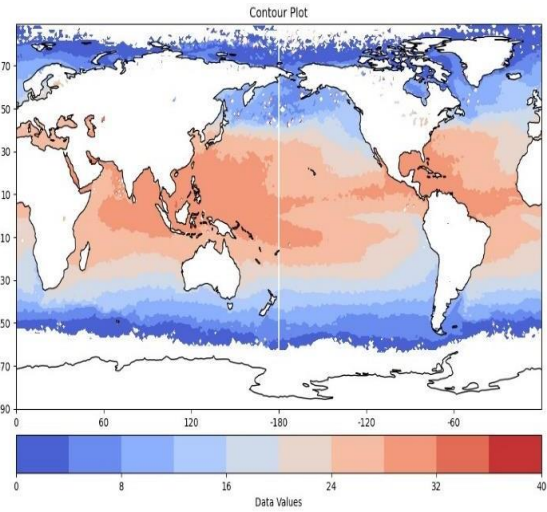
Fig 3.2 shows precipitation over the Indian Ocean

CHAPTER 4: ANALYSIS AND CONCLUSION

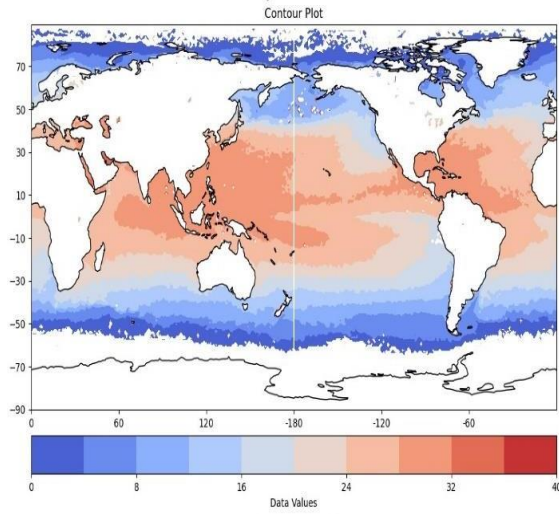
4.1 Sea Surface Temperature



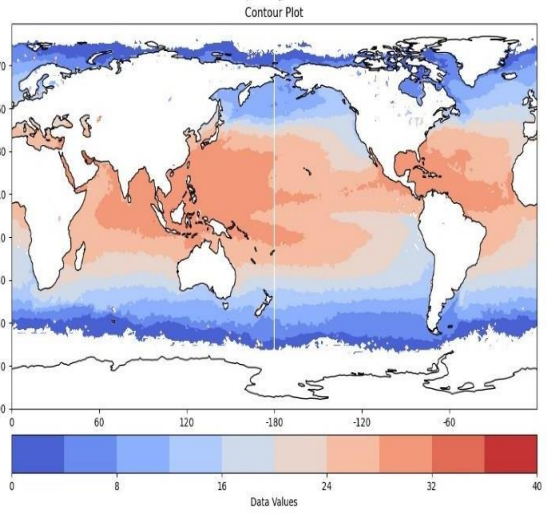
a) June 2010



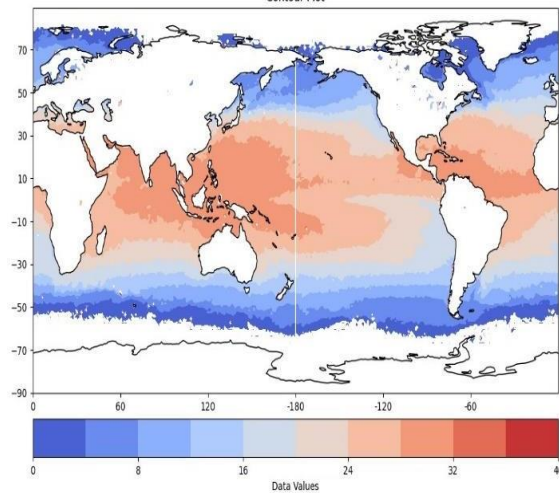
b) July 2010



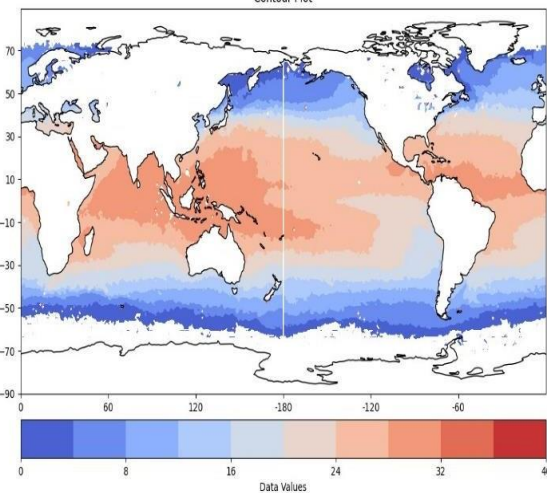
c) August 2010



d) September 2010



e) October 2010



f) November 2010

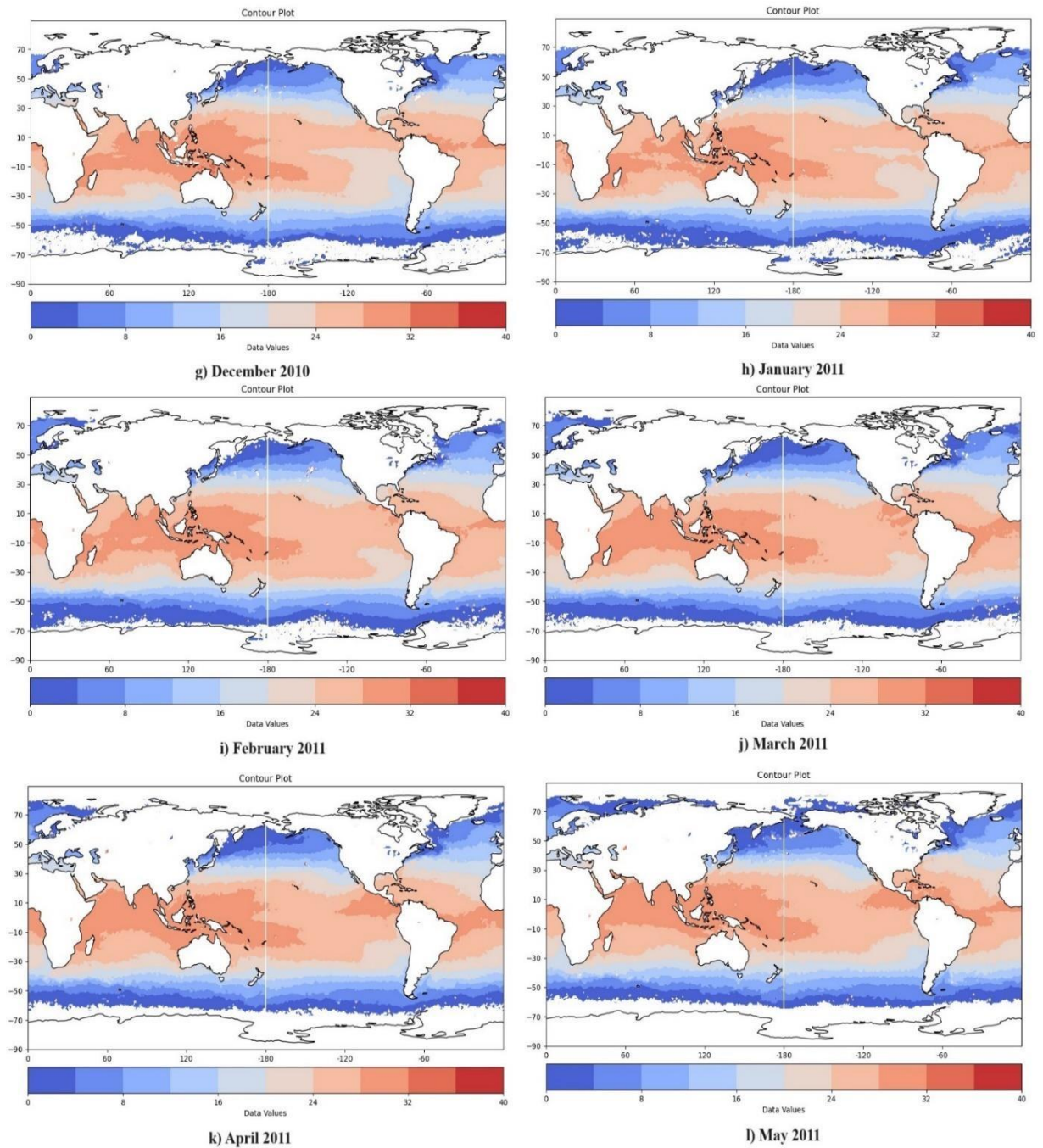


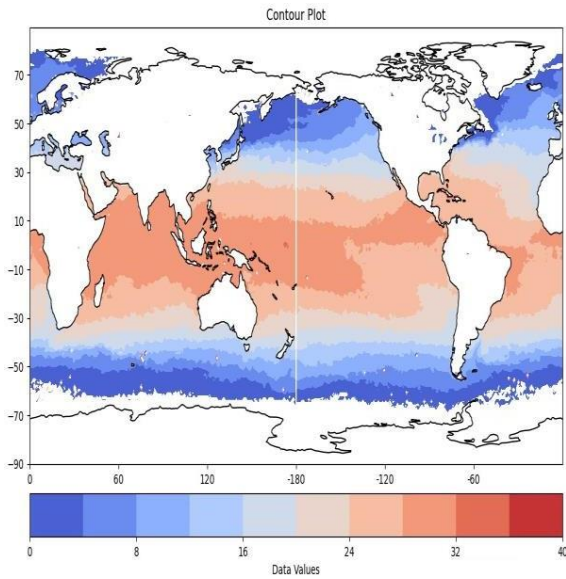
Figure 4.1.1 Monthly Mean of Sea Surface Temperature Over a Strong La-Nina Year 2010-2011.

Fig 4.1.1 and Fig 4.1.2 is a set of contour plots of sea surface temperature of the year 2010 June to 2011 May and April 2015 to March 2016. The maximum temperature observed is 0° C and the maximum temperature observed is 40 ° C. Sea surface temperatures, up to 20° C, are denoted by blue contours and temperatures beyond 20° C are donated by red contours.

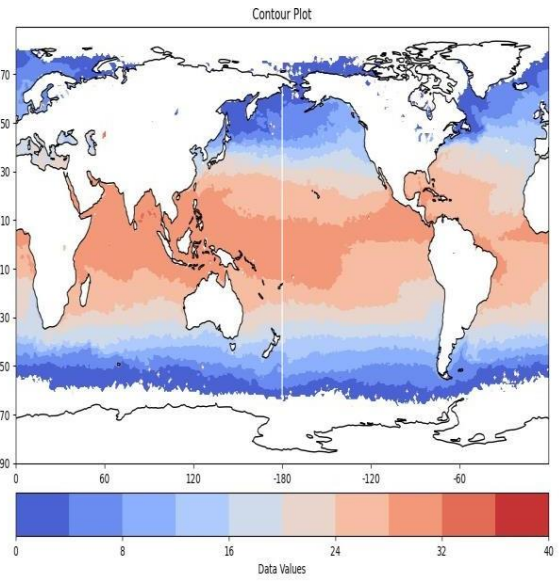
Fig 4.1.1 is a set of contour plots of sea surface temperature for the year 2010-2011. The year 2010 June to 2011 May was a year that experienced a strong La-Nina phase. The temperature around the central and eastern Pacific Ocean is observed to be around 24° C. The La-Nina phase started around

June 2010. The sea surface temperature around the central and eastern Pacific Ocean decreases from June 2010 to May 2010 also during this time the ONI values are observed to be the lowest. The temperature of the Pacific Ocean is decreasing from 24° C to 20°C. Around October and November 2010, the temperature of the major parts of central and eastern parts of the Pacific Ocean was around 20° C. The sea surface temperature again started increasing around May 2011.

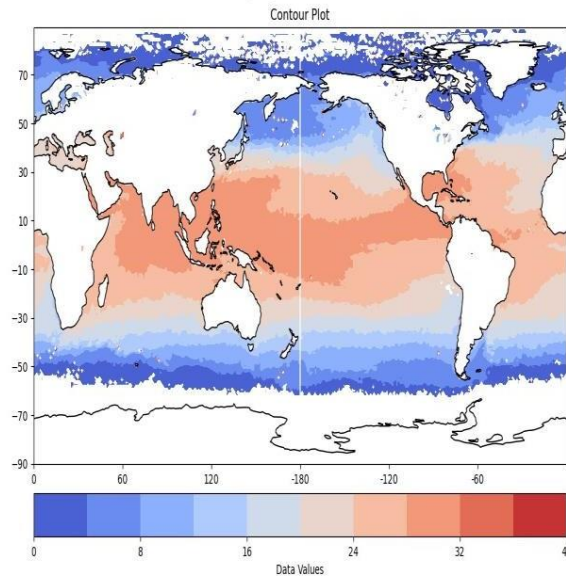
In June 2010 the temperature around the Central Pacific Ocean was about 26° C. During July 2010 the temperature around the southern tip of North America decreased. The decrease in temperature further continues in August and September. During October, the temperature of the Central Pacific decreases to around 24° C. In November 2010 the temperature around the southern tip of North America was also observed to decrease extremely. In December 2010 the temperature of major parts of the central and eastern Pacific Ocean is observed to be around 22-24° C. The drop in temperature is even observed during December as during this time this region experiences the summer season. The temperature further decreased in January 2011. In February the temperature is observed to slightly increase as March approaches the temperature further increases. In April 2011 the temperature along the tip of North America increased it is again observed to be around 26 ° C. The temperature remains constant till June however in July the temperature around the central and eastern part of the Pacific Ocean is further observed to increase.



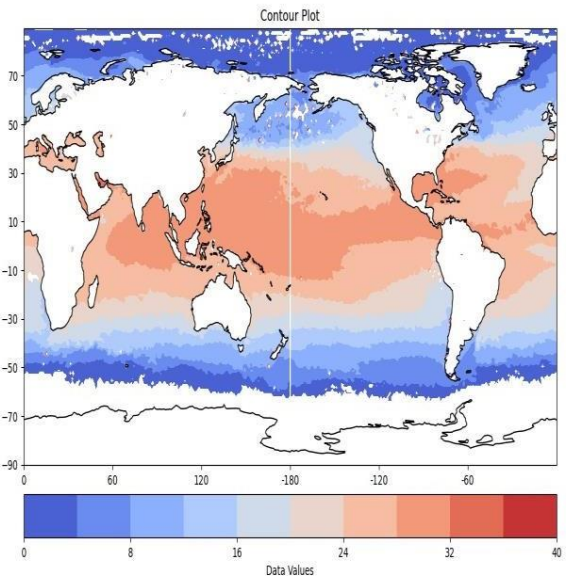
a) April 2015



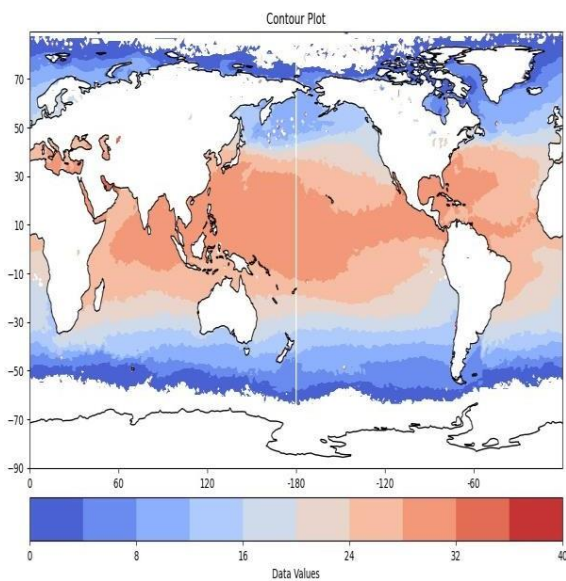
b) May 2015



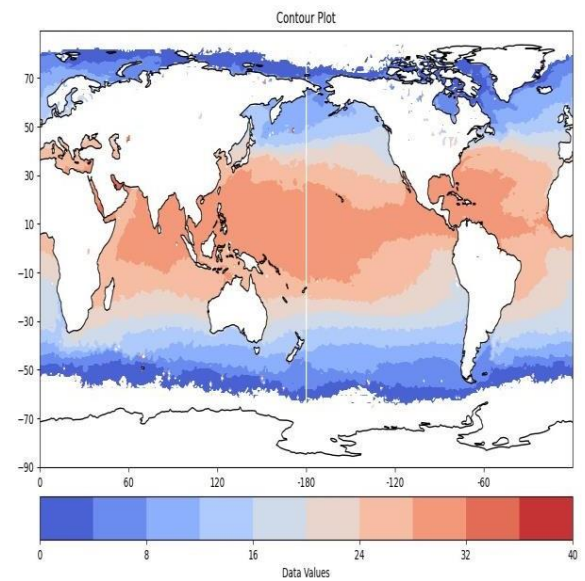
c) June 2015



d) July 2015



e) August 2015



f) September 2015

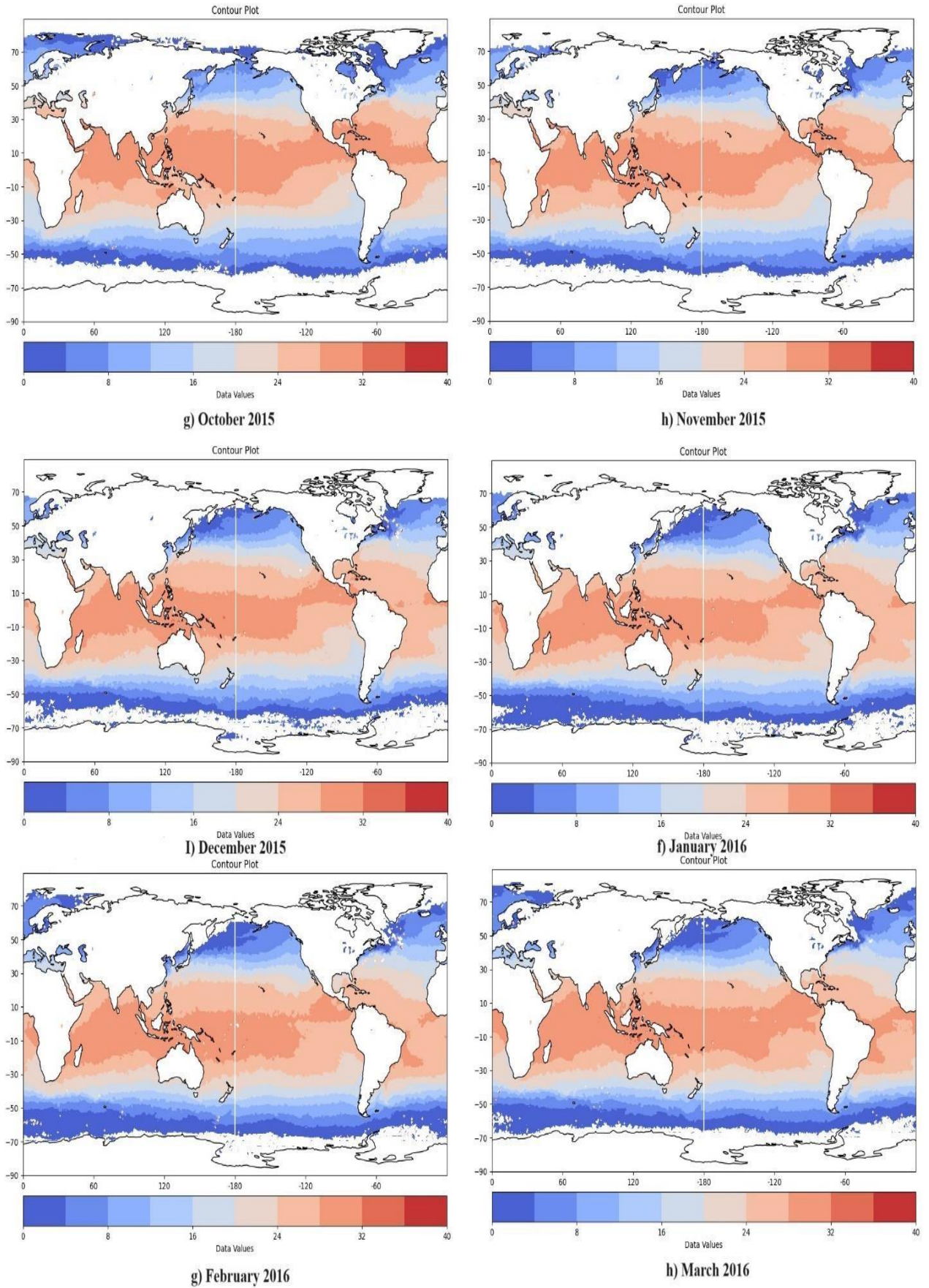


Figure 4.1.2 Monthly Mean Of Sea Surface Temperature Over A Super Strong El-Niño Year 2015-2016.

Fig 4.1.2 is a set of contour plots of sea surface temperature for the year 2015-2016. The year 2015-16 was a year that experienced a strong El-Nino phase of the ENSO cycle. The temperature around the central and eastern Pacific Ocean is observed to be around 26 ° C. The El-Nino phase started around April 2015. The temperature around the central and eastern Pacific Ocean increased from April 2015 to November 2015. The temperature around this region was around 24 ° C the temperature increased to 28 ° C also during this time the ONI values were observed to be the highest. The temperature then decreases from December 2015 to March 2016. In the months of April and May 2015, the temperature around the central and eastern Pacific oceans was around 28 ° C. The intensity of the temperature continues to increase during the months of June, July, and August. During these months the temperature along the coast of China. During the next three months, the temperature along the coast of China decreases. In the month of December, the sea surface temperature is also observed to decrease along the coast of the southern part of North America. Further in the month of January 2016 the temperature of major regions of the central Pacific Ocean decreased and continued to decrease till the month of February 2016. However, during the month of March, the temperature increases in this region.

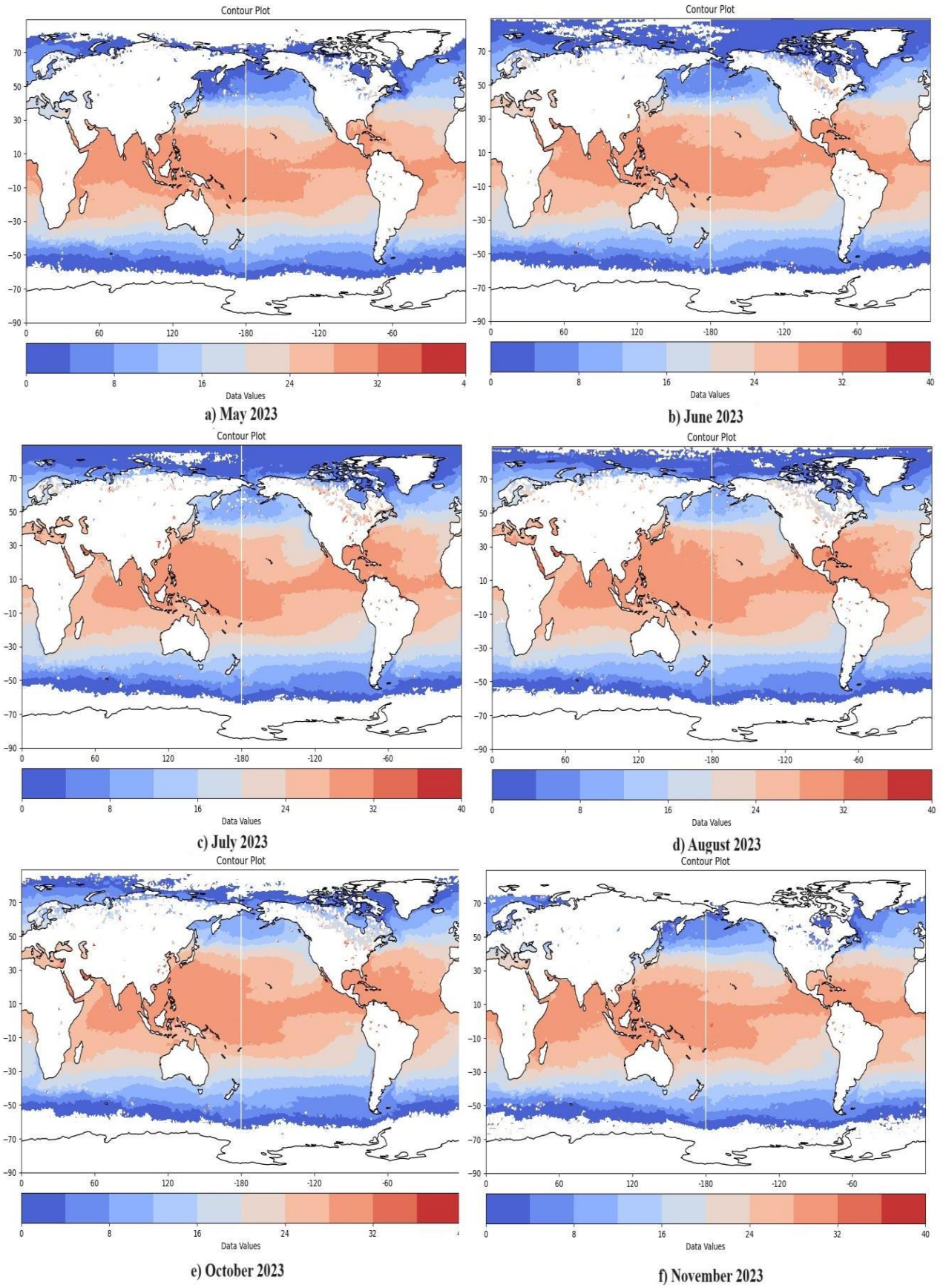


Figure 4.1.3 Monthly Mean of Sea Surface Temperature Over a Strong El-Nino Year 2023.

Fig 4.1.2 is a set of contour plots of sea surface temperature for the year 2023. The year 2023 was a year that experienced a strong El-Nino phase of the ENSO cycle. The temperature around the central and eastern Pacific Ocean is observed to be around 26°C . The El-Nino phase started around March 2023. The temperature around the central and eastern Pacific Ocean increased from May 2023 to November 2023. The temperature around this region was around 24°C the temperature increased to 28°C also during this time the ONI values were observed to be the highest. In the month of March, the sea surface temperature around the central and eastern Pacific Ocean is observed to be around $20\text{-}30^{\circ}\text{C}$. In April the temperature in the eastern part increases. In May the temperature further increases along the eastern part of the Pacific Ocean and also along the southern tip of North America. An increase in the trend of temperature is observed through June, July, and August. The Data for September was not available. During October the sea surface temperature is slightly observed to decrease compared to August. In November the sea surface temperature further decreases towards the coast of North America.

4.2 Sea Surface Anomaly

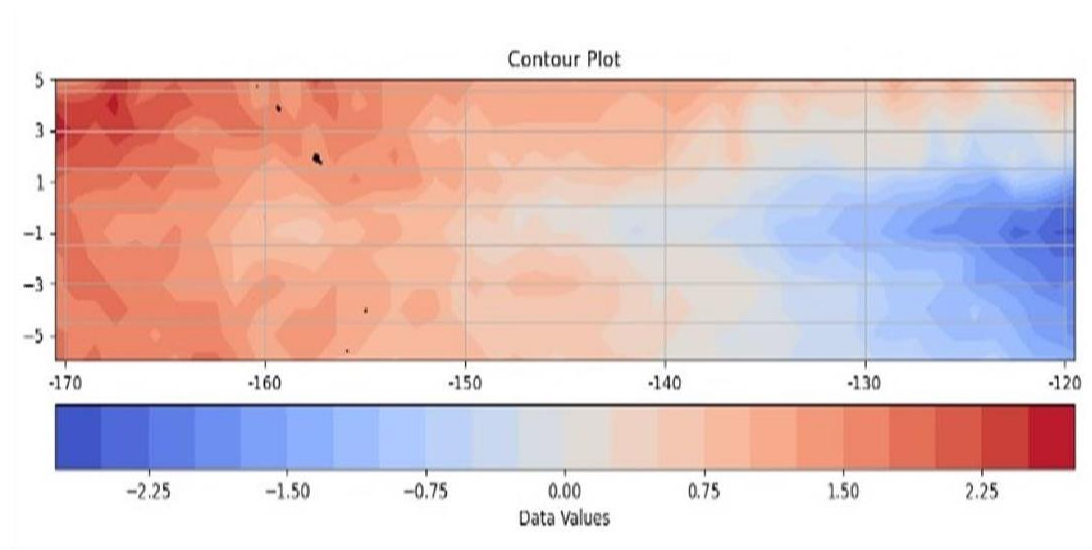


Figure 4.2.1 Sea Surface Temperature Anomaly over the Niño 3.4 region during August 2012.

Figures 4.2.1, 4.2.2, 4.2.3, 4.2.4, and 4.2.5 are the sea surface temperature anomaly plots of the Niño 3.4 region. The Niño 3.4 region is a segment of the equatorial Pacific Ocean spanning from approximately 120°W to 170°W longitude and 5°N to 5°S latitude. Niño-3.4, located in the central Pacific, The Niño 3.4 region serves as a key indicator for monitoring and predicting El Niño and La Niña events. In these plots, the positive values of SSTA are denoted by red contours and the negative values of SSTA are denoted by blue color contours.

Fig 4.2.1 is the SSTA plot of August 2012 which is the neutral phase of ENSO. The value of ONI during this month is observed to be 0.07553. In this region, the SSTA values between longitude -170 and -160 are 2.25 units. The SSTA values decrease between the -160 and -130 longitude. The SSTA values are extremely low between the -130 and -120 longitude which is around -1.5 to -2.25 units. Over all a large contrast is seen between the two ends.

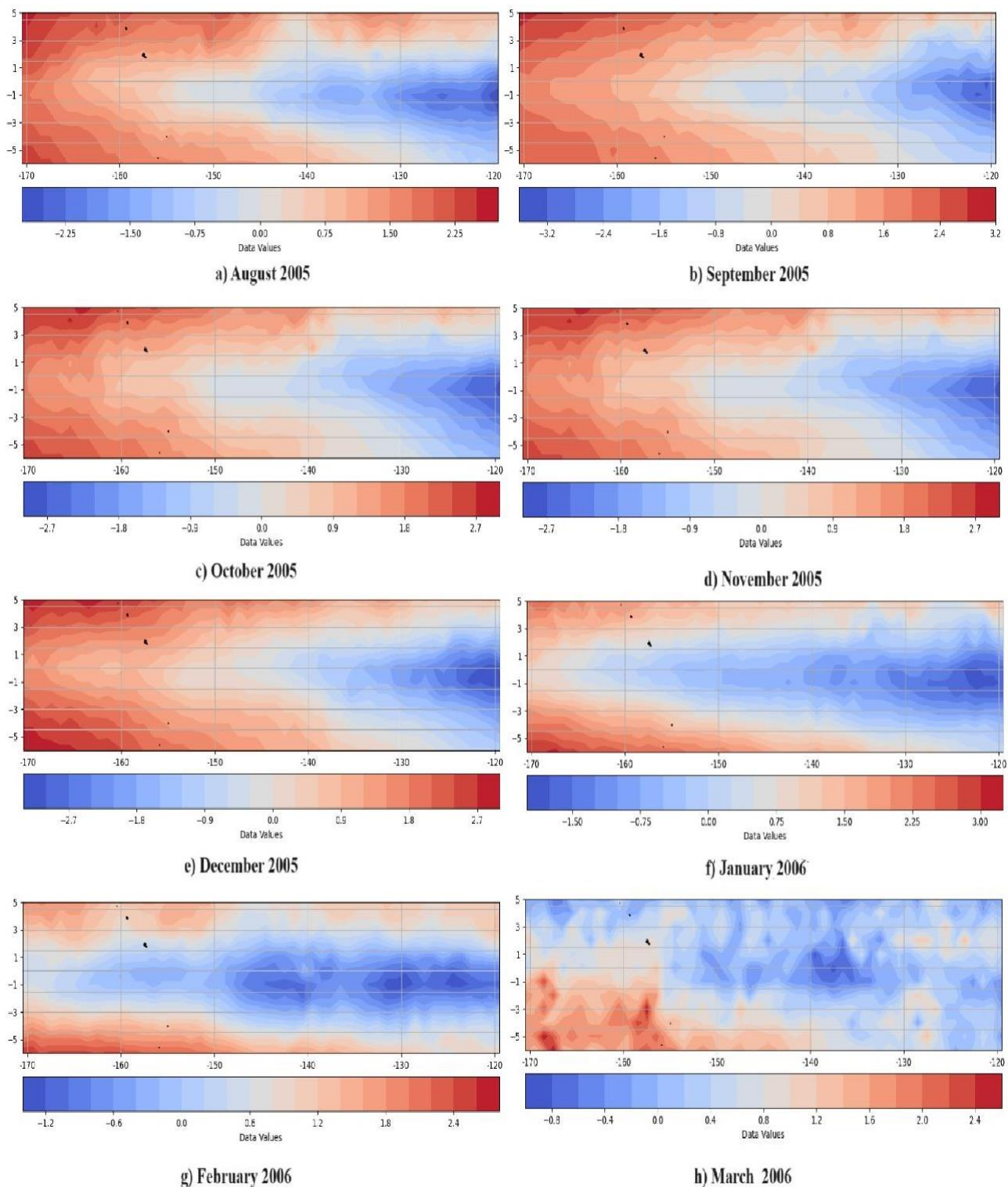
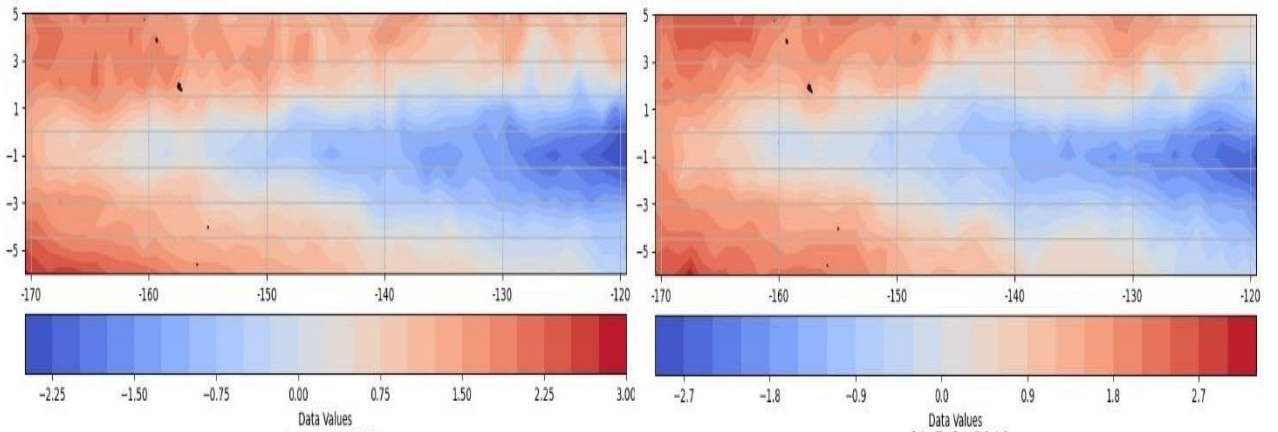


Figure 4.2.2 Sea Surface Temperature Anomaly over the Niño 3.4 region during Weak LaNiña phase observed from August 2005 to February 2006.

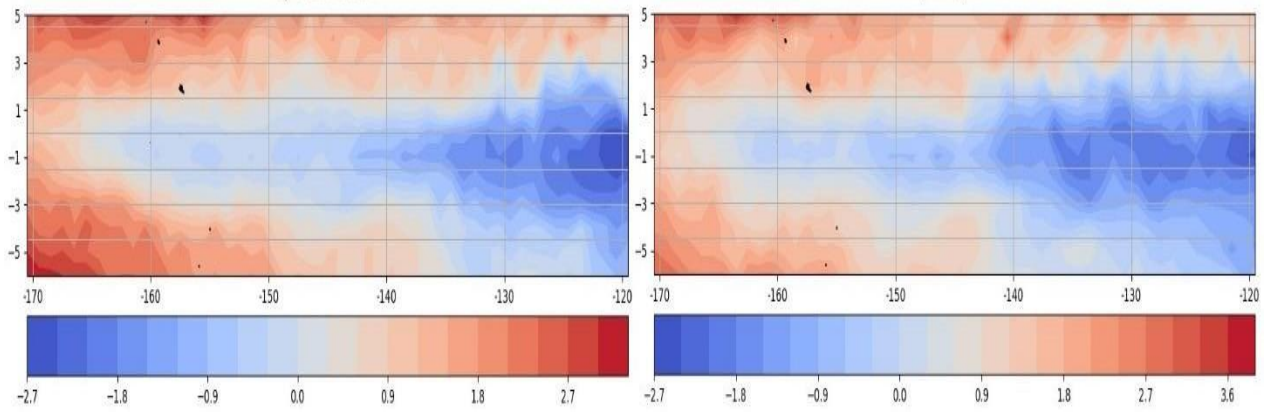
Figure 4.2.2 is a series of SSTA plots from August 2005 to February 2006. This period is observed to be a weak La-Niña phase of the ENSO cycle. During this phase the SSTA values between -170 and -

It is observed to have very high positive values. The intensity of the contours increases as the intensity of the phenomenon increases. The SSTA values between -160 and -130 are mostly between -0.75 and +1.50. The SSTA values between -130 and -120 longitude are observed to be very low, around -1.50. The intensity of the contours increases as the intensity of the phenomenon increases. The highest ONI value was observed during December 2005 which is -1.03372 units. In the month of August, the SSTA the SSTA values are higher between the -170 and -150 longitudes and lower values are observed between -140 and -120 longitudes. The conditions remain the same for the month of September. In November SST is observed to be high between -170 to -150 and lower values are observed to be between -150 and -120. In December, the condition is observed to be similar to that in the month of September. In January values of SSTA increased. The SST values further decreased in the month of February. In March, the SSTA values tend to increase again.



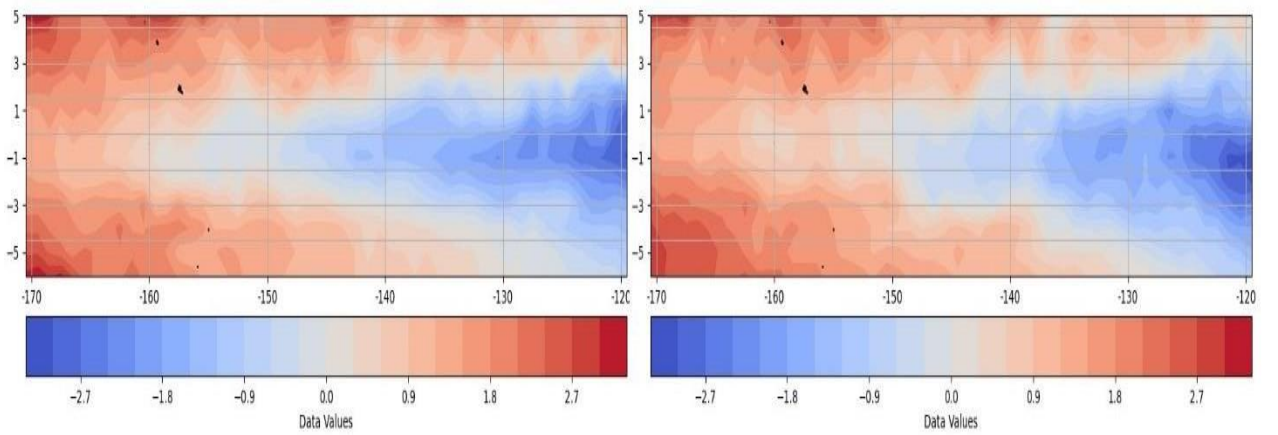
a) June 2010

b) July 2010



c) August 2010

d) September 2010



e) October 2010

f) November 2010

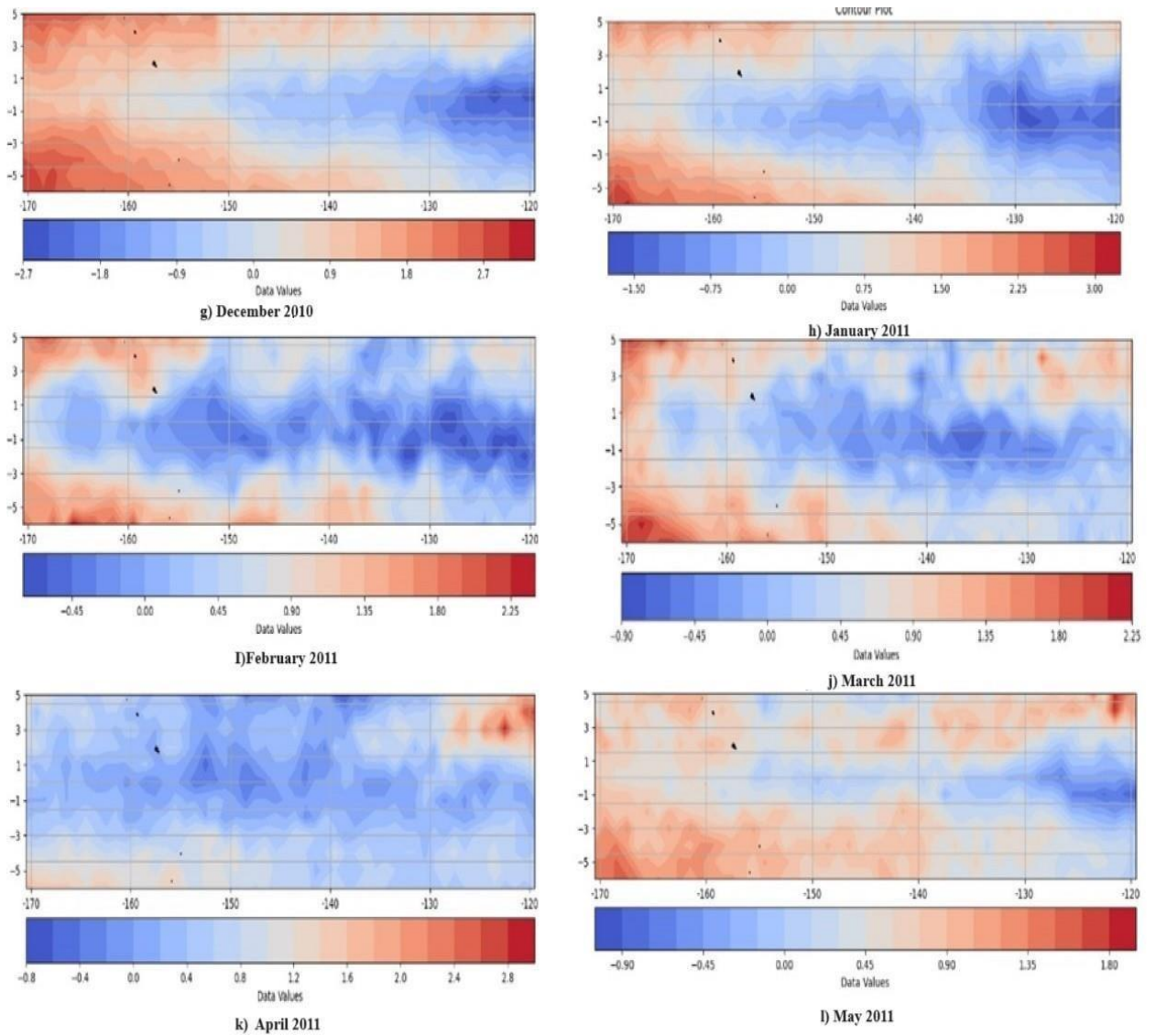
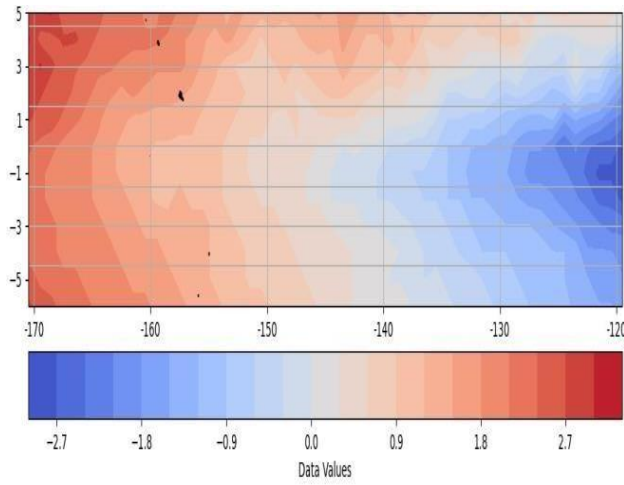


Figure 4.2.3 Sea Surface Temperature Anomaly over the Niño 3.4 region during super strong La Niña phase observed from June 2010 to May 2011.

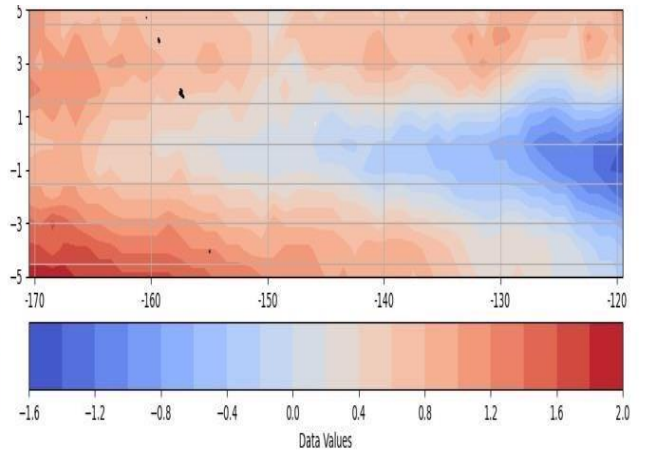
Figure 4.2.3 is a series of SSTA plots from June 2010 to May 2011. This period is observed to be a super strong La-Niña phase of the ENSO cycle. During this phase the SSTA values between -170 and -160

It is observed to have very highly positive values. The intensity of the contours decreases as the intensity of the phenomenon increases. The SSTA values between -160 and -130 are mostly between -0.45 and $+0.50$. The SSTA values between -130 and -120 longitude are observed to be very low, around -1.50 . The intensity of the contours increases as the intensity of the phenomenon increases. The highest ONI value was observed during November 2010 which is -2.14016 units. Overall, most

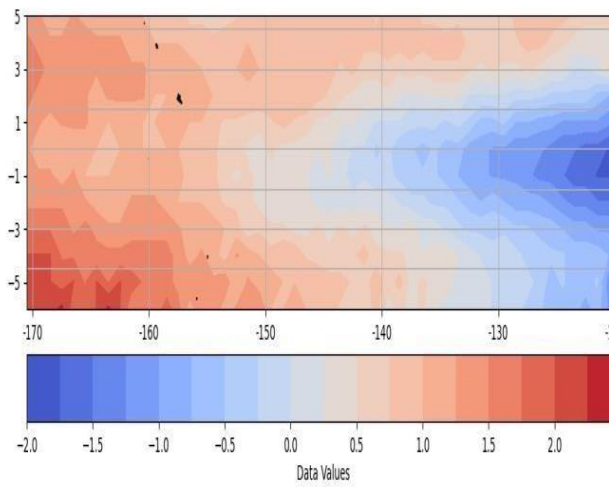
parts of the plots are covered by negative SSTA values. In the month of June, the SSTA the SSTA values are higher between the -170 and -150 longitudes and lower values are observed between -140 and -120 longitudes. Similar temperature patterns are observed in July and August. In September the major part of the maps is covered by the lower SSTA values in November and December major part is covered by higher SSTA values. In January the major part of the maps is covered by the lower SSTA values they are majorly observed between the -160 and -120 longitude. In February the lower SSTA values are seen throughout the Nino 3.4 region except around the -170 longitude. Similar conditions are seen in March. In April the lower SSTA values are seen throughout the Nino 3.4 region even around the -170 latitude.in April the major values are observed between -0.45 units and 0.90.



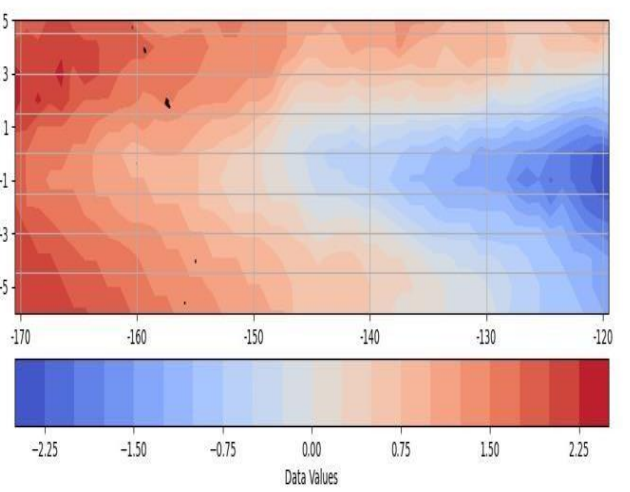
a) April 2006



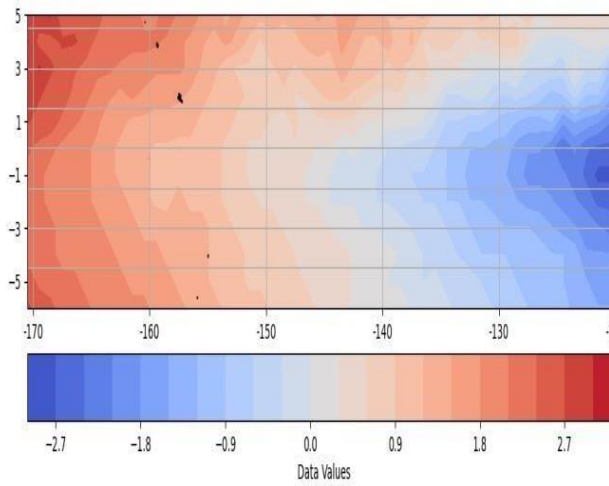
b) May 2006



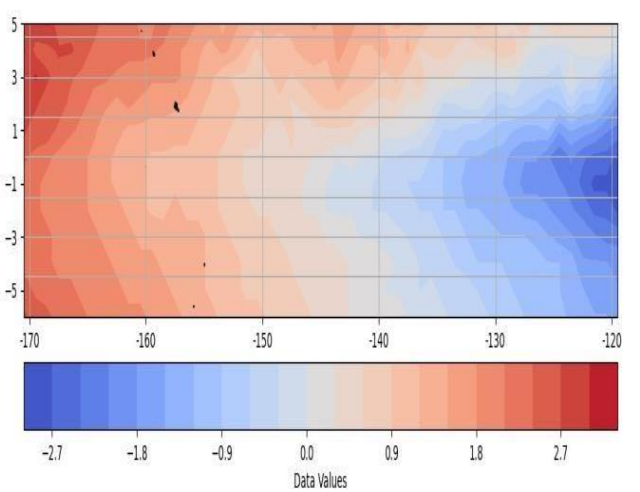
c) June 2006



d) July 2006



e) August 2006



f) September 2006

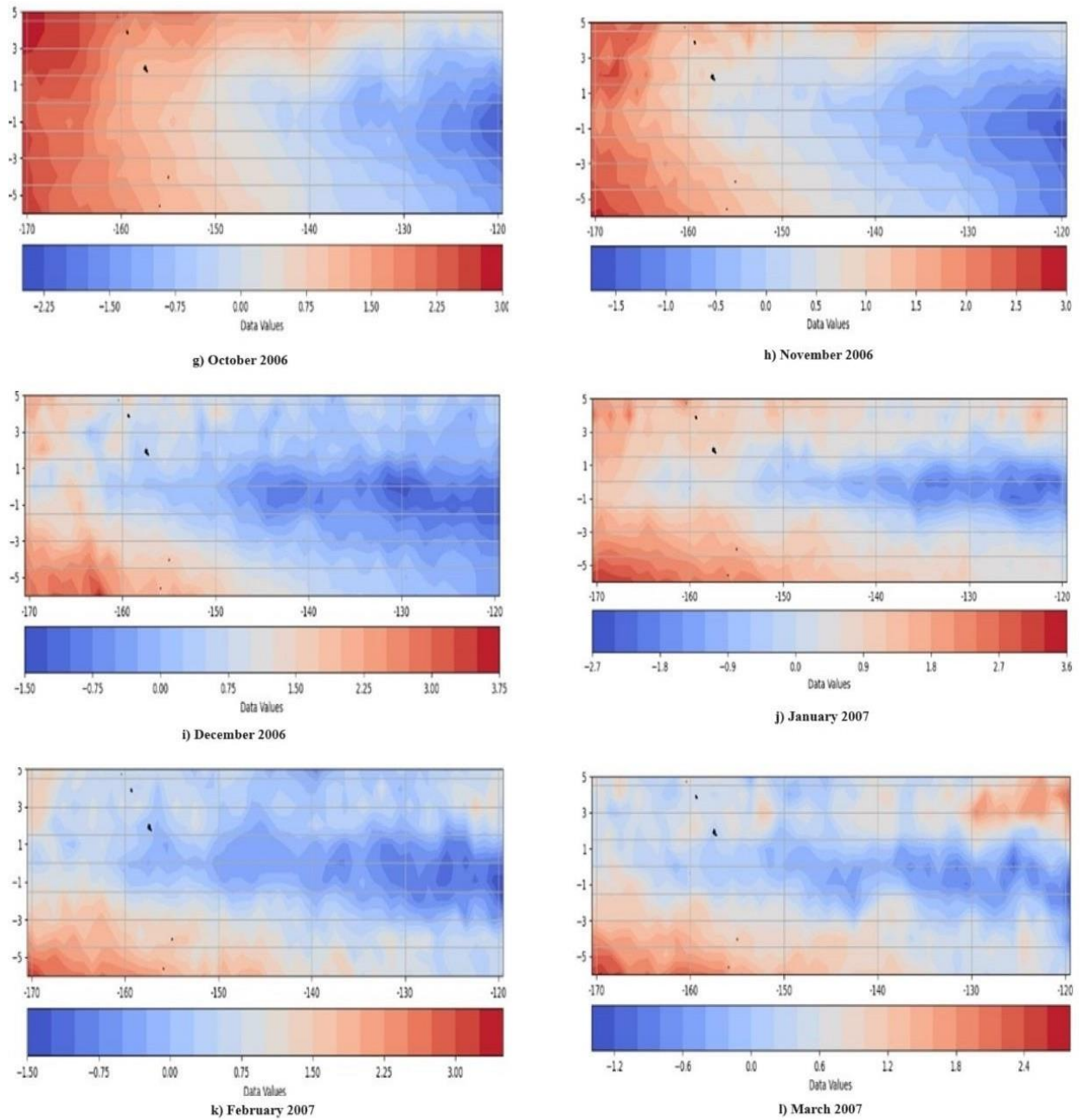
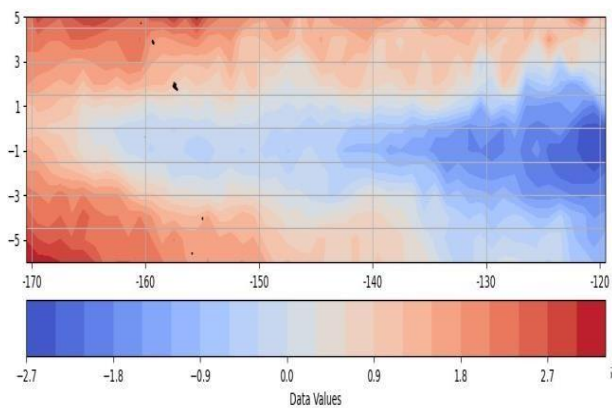


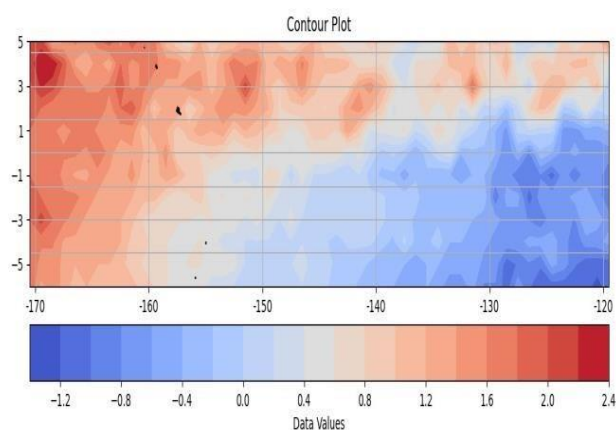
Figure 4.2.4 Sea Surface Temperature Anomaly over the Niño 3.4 region during weak El-Niño phase observed from April 2006 to March 2007.

Figure 4.2.4 is a series of SSTA plots from April 2006 to March 2007. This period is observed to be a Weak El-Niño phase of the ENSO cycle. During this phase the SSTA values between 170° and 120°

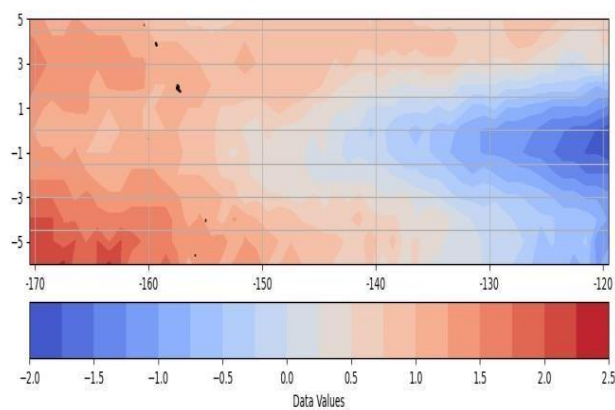
is observed to have very highly positive values. The intensity of the contours increases as the intensity of the phenomenon increases. The SSTA values between -160 and -130 are mostly between -0.75 and +1.50. The SSTA values between -130 and -120 longitude are observed to be very low, around -1.50. The intensity of the contours decreases as the intensity of the phenomenon increases. The highest ONI value was observed during May 2006 which is 0.67705 units. Overall, most parts of the plots are covered by positive SSTA values. In April major regions in covered by lower values SSTA values the higher SSTA values are only observed along the -170 longitude. In May the intensity of the higher values increases around the -170 longitude, whereas in June it rapidly decreases. Similar conditions are observed in July and the intensity of values increases in August. Similar conditions are observed in September October, November, December, and January. In February and March, the lower values of SSTA cover more than 50% of the region.



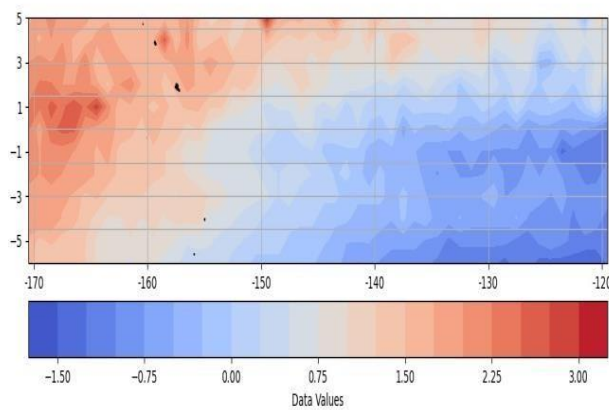
a) April 2015



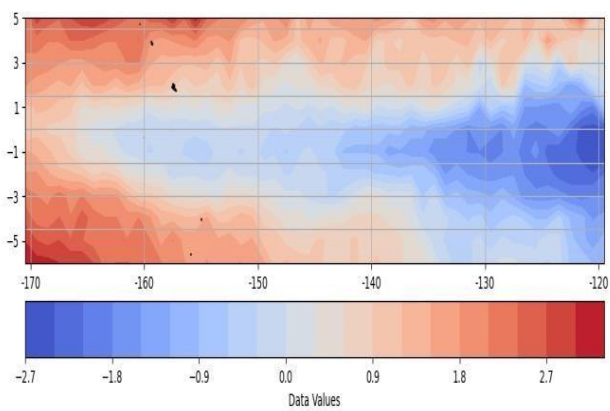
b) May 2015



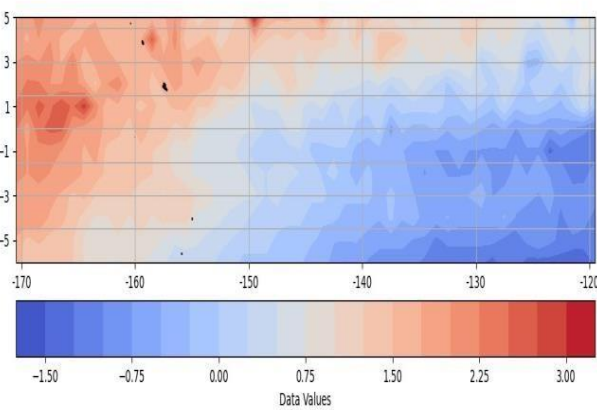
c) June 2015



d) July 2015



e) August 2015



f) September 2015

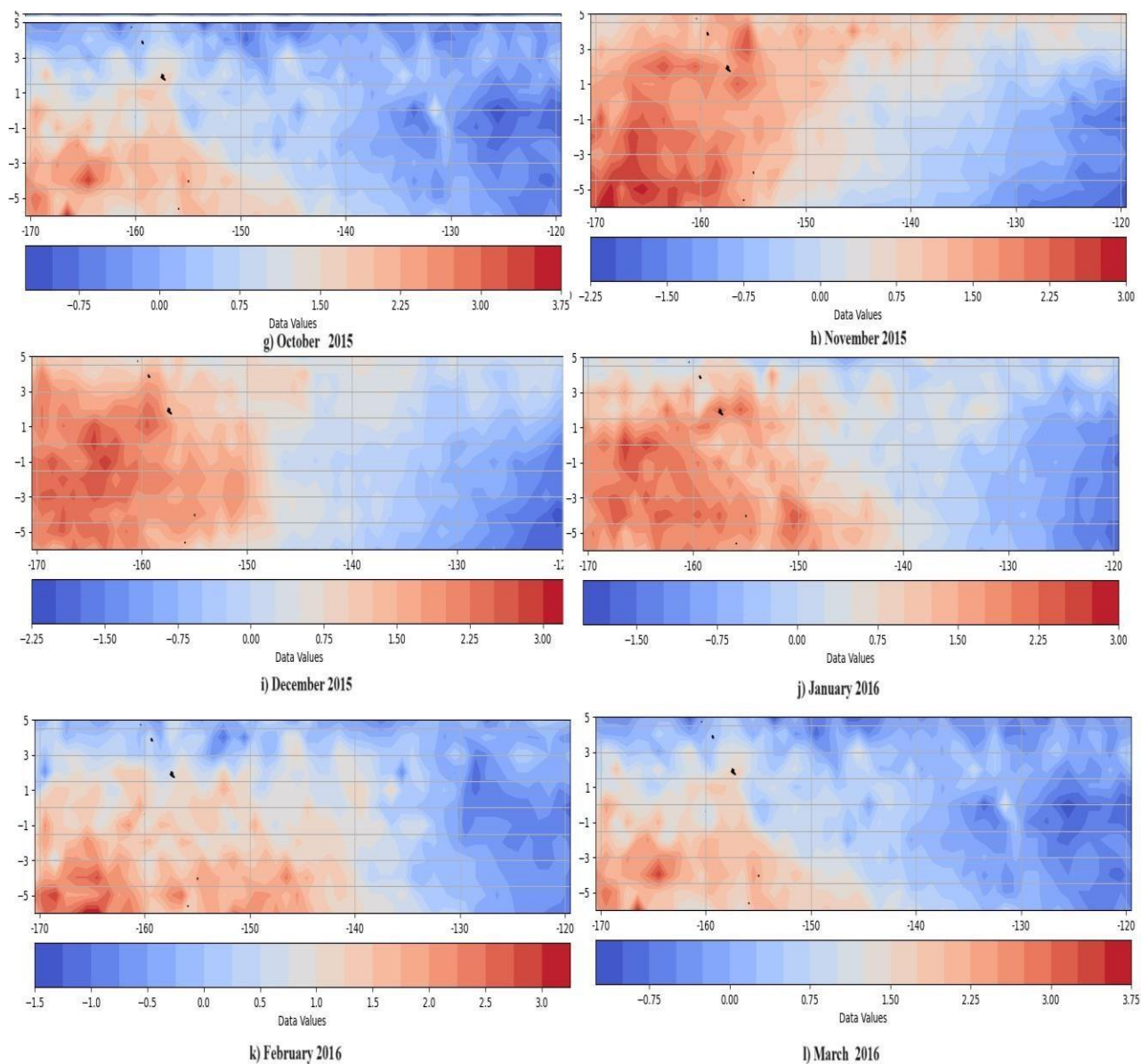


Figure 4.2.5 Sea Surface Temperature Anomaly over the Niño 3.4 region during the super strong El-Niño phase observed from April 2015 to March 2016.

Fig 4.2.5 is a series of SSTA plots from April April 2015 to March 2016. This period is observed to be a super strong El-Niño phase of the ENSO cycle. During this phase, the SSTA values between -170 and -160 are observed to have very highly positive values. The intensity of the contours increases as the intensity of the phenomenon increases. The SSTA values between -160 and -130 are mostly between -0.75 and +2.250. The SSTA values between -130 and -120 longitude are observed to be very low, around -1.50. The intensity of the contours decreases as the intensity of the phenomenon increases. The highest ONI value was observed during October 2015 which is +2.24068 units. After

October 2015 the positive values decreased between the -170 and -160 longitude. Overall, most parts of the plots are covered by positive SSTA values. In April major regions in covered by lower values SSTA values the higher SSTA values are only observed along the -170 longitude. In May the intensity of the higher values increases around the -170 longitude, whereas in month of June it rapidly decreases. Similar conditions are observed in the month of July and the intensity of values increases in the month of August. Similar conditions are observed in the month of September October, November, December and January . In the month of February and March the lower values of SSTA cover more than 50% of the region.

4.3 Oceanic Nino Index

4.3.1 Table showing monthly variation of the Oceanic Nino Index.

Y/M	Mean	SST Anomaly	ONI	Y/M	Mean	SST Anomaly	ONI
1982/1	26.61462	-0.4151609	-0.21502	1985/8	26.57213	-0.4576537	-0.62304
1982/2	26.60875	-0.4210351	0.221016	1985/9	26.35125	-0.6785351	-0.75003
1982/3	27.22091	0.19112839	0.822726	1985/10	26.29684	-0.7329421	-0.82343
1982/4	27.92274	0.89295531	1.225888	1985/11	26.19119	-0.8385992	-0.95668
1982/5	28.41388	1.38409314	1.153431	1985/12	26.13103	-0.8987594	-0.9913
1982/6	28.4304	1.40061557	0.949424	1986/1	25.89712	-1.1326697	-0.80386
1982/7	27.70537	0.67558352	0.812202	1986/2	26.08732	-0.9424614	-0.28193
1982/8	27.80186	0.7720739	1.130375	1986/3	26.69335	-0.3364357	0.208372
1982/9	28.01873	0.9889489	1.392993	1986/4	27.4629	0.43311557	0.540194
1982/10	28.65989	1.63010275	1.715188	1986/5	27.55822	0.52843609	0.508164
1982/11	28.58971	1.55992647	1.791251	1986/6	27.68881	0.65902903	0.376898
1982/12	28.98532	1.95553544	1.871171	1986/7	27.36681	0.33702583	0.260877
1983/1	28.88808	1.85829186	1.735162	1986/8	27.16442	0.13463801	0.326134
1983/2	28.82947	1.79968609	1.68827	1986/9	27.34075	0.31096814	0.511524
1983/3	28.57729	1.5475066	1.671326	1986/10	27.56258	0.53279506	0.633206
1983/4	28.7474	1.71761878	1.6459	1986/11	27.72059	0.69080788	0.734382
1983/5	28.77864	1.74885275	1.104292	1986/12	27.7058	0.67601621	0.822603
1983/6	28.50101	1.47122855	0.373384	1987/1	27.86611	0.8363207	1.05857
1983/7	27.12258	0.09279506	-0.3079	1987/2	27.98526	0.95547134	1.343837
1983/8	26.58591	-0.4438716	-0.7392	1987/3	28.4137	1.38391686	1.58116
1983/9	26.45716	-0.5726216	-1.0707	1987/4	28.72191	1.69212198	1.748511
1983/10	25.82869	-1.2010992	-1.36173	1987/5	28.69723	1.6674425	1.755258
1983/11	25.59139	-1.4383908	-1.41635	1987/6	28.91575	1.88596814	1.70436
1983/12	25.58407	-1.4457146	-1.11391	1987/7	28.74215	1.71236237	1.526438
1984/1	25.66484	-1.3649453	-0.70607	1987/8	28.54454	1.51475019	1.30694
1984/2	26.4987	-0.5310831	-0.11954	1987/9	28.38199	1.35220211	1.132053
1984/3	26.80761	-0.2221729	0.155071	1987/10	28.08365	1.05386878	0.906716
1984/4	27.42441	0.39462198	0.146278	1987/11	28.01987	0.99008673	0.670872
1984/5	27.32255	0.29276301	-0.09301	1987/12	27.70598	0.6761925	0.425434
1984/6	26.78123	-0.2485511	-0.40078	1988/1	27.37612	0.34633673	0.324184
1984/7	26.70654	-0.3232466	-0.50786	1988/2	27.28356	0.25377262	0.336112
1984/8	26.39925	-0.6305383	-0.76272	1988/3	27.40223	0.3724425	0.125867
1984/9	26.45998	-0.5698011	-1.0536	1988/4	27.41191	0.38212198	-0.25865
1984/10	25.94197	-1.0878139	-1.46816	1988/5	26.65282	-0.3769646	-0.82371
1984/11	25.52659	-1.5031985	-1.58586	1988/6	26.24867	-0.7811152	-1.24197
1984/12	25.21631	-1.813471	-1.50955	1988/7	25.71673	-1.3130543	-1.49599
1985/1	25.58888	-1.4409069	-1.13156	1988/8	25.39804	-1.6317402	-1.78857
1985/2	25.75551	-1.2742722	-0.70099	1988/9	25.4866	-1.5431825	-2.08852
1985/3	26.35029	-0.6794966	-0.22897	1988/10	24.83901	-2.1907787	-2.41466
1985/4	26.88059	-0.1491921	-0.02996	1988/11	24.49817	-2.531612	-2.45834
1985/5	27.17155	0.14176942	-0.09226	1988/12	24.50821	-2.5215799	-2.15311
1985/6	26.94732	-0.0824614	-0.29207	1989/1	24.70795	-2.3218364	-1.64587
1985/7	26.6937	-0.3360831	-0.49076	1989/2	25.41388	-1.6159069	-0.95825

1989/3	26.0299	-0.9998812	-0.38059	1993/4	28.56229	1.5325066	1.485322
1989/4	26.77082	-0.2589678	-0.03767	1993/5	28.76149	1.73170531	1.179676
1989/5	27.14686	0.11707391	-0.02901	1993/6	28.22154	1.19175339	0.569986
1989/6	27.05867	0.0288848	-0.28841	1993/7	27.64536	0.61556996	0.167091
1989/7	26.79679	-0.2329902	-0.53345	1993/8	26.93242	-0.0973652	-0.04035
1989/8	26.36865	-0.6611312	-0.68586	1993/9	27.01285	-0.0169325	-0.01294
1989/9	26.32356	-0.7062274	-0.70055	1993/10	27.02303	-0.0067562	-0.07881
1989/10	26.33955	-0.6902338	-0.66394	1993/11	27.01466	-0.0151216	-0.18639
1989/11	26.3246	-0.7051857	-0.57829	1993/12	26.81522	-0.2145607	-0.28336
1989/12	26.43338	-0.5964037	-0.3553	1994/1	26.7003	-0.3294806	-0.10397
1990/1	26.59649	-0.4332947	0.003236	1994/2	26.72375	-0.3060351	0.310076
1990/2	26.99358	-0.0362066	0.462205	1994/3	27.35338	0.32359634	0.76819
1990/3	27.50899	0.47920901	0.809426	1994/4	27.94245	0.91266685	0.984334
1990/4	27.9734	0.94361237	0.839109	1994/5	28.09809	1.06830788	0.812699
1990/5	28.03524	1.00545532	0.60077	1994/6	28.00181	0.97202583	0.556262
1990/6	27.59804	0.5682598	0.283169	1994/7	27.42755	0.39776301	0.250979
1990/7	27.25838	0.22859634	0.031054	1994/8	27.32878	0.29899698	0.284579
1990/8	27.08244	0.05265083	-0.0428	1994/9	27.08596	0.05617647	0.45912
1990/9	26.8417	-0.1880864	-0.13591	1994/10	27.52835	0.49856429	0.722539
1990/10	27.03683	0.00704186	-0.09617	1994/11	27.8524	0.82261878	0.722309
1990/11	26.80311	-0.2266761	-0.09099	1994/12	27.87622	0.84643288	0.602774
1990/12	26.9609	-0.0688876	-0.02074	1995/1	27.52766	0.49787519	0.542667
1991/1	27.05239	0.02260275	0.096246	1995/2	27.4938	0.46401301	0.683623
1991/2	27.01385	-0.0159389	0.412891	1995/3	27.6959	0.66611237	0.779366
1991/3	27.31186	0.28207391	0.856481	1995/4	27.95053	0.92074378	0.765242
1991/4	28.00232	0.97253865	1.19272	1995/5	27.78103	0.75124057	0.477565
1991/5	28.34462	1.31483032	1.164184	1995/6	27.65353	0.62374057	0.033805
1991/6	28.32058	1.29079186	0.874723	1995/7	27.0875	0.05771493	-0.48893
1991/7	27.91671	0.88692968	0.48131	1995/8	26.44974	-0.5800415	-0.84002
1991/8	27.47623	0.44644891	0.393944	1995/9	26.08532	-0.9444646	-1.06672
1991/9	27.14034	0.11055147	0.510295	1995/10	26.03423	-0.9955543	-1.19709
1991/10	27.65462	0.62483032	0.913746	1995/11	25.76963	-1.2601537	-1.26152
1991/11	27.82529	0.79550339	1.149152	1995/12	25.69421	-1.3355703	-1.19821
1991/12	28.35069	1.32090403	1.372069	1996/1	25.84095	-1.1888396	-0.85716
1992/1	28.36083	1.33104827	1.525754	1996/2	25.95957	-1.0702178	-0.33902
1992/2	28.49404	1.46425339	1.747832	1996/3	26.71737	-0.3124133	0.143361
1992/3	28.81175	1.78196173	1.879638	1996/4	27.39537	0.36558352	0.358041
1992/4	29.02707	1.99728224	1.493564	1996/5	27.4067	0.37691365	0.253292
1992/5	28.88946	1.85967006	0.847042	1996/6	27.36141	0.33162519	0.007475
1992/6	27.65353	0.62374057	0.033805	1996/7	27.08112	0.05133672	-0.30133
1992/7	27.0875	0.05771493	-0.45982	1996/8	26.66925	-0.3605383	-0.54581
1992/8	26.44974	-0.5800415	-0.81091	1996/9	26.435	-0.5947851	-0.66187
1992/9	26.17264	-0.8571408	-1.03762	1996/10	26.34769	-0.6820928	-0.76341
1992/10	26.03423	-0.9955543	-1.19709	1996/11	26.32104	-0.7087434	-0.85357
1992/11	25.76963	-1.2601537	-0.94186	1996/12	26.13038	-0.8994004	-0.81613
1992/12	25.69421	-1.3355703	-0.50858	1997/1	26.07723	-0.9525575	-0.47633
1993/1	26.79992	-0.2298652	0.157256	1997/2	26.43337	-0.5964197	0.172047
1993/2	27.06949	0.03970211	0.744713	1997/3	27.14978	0.11999057	0.86818
1993/3	27.69171	0.66192967	1.308714	1997/4	28.02236	0.9925707	1.425712

1997/5	28.52176	1.49197775	1.685135	2001/6	27.65056	0.62077583	0.248725
1997/6	28.82237	1.79258672	1.766417	2001/7	27.28885	0.25906108	-0.10515
1997/7	28.80063	1.77083993	1.786793	2001/8	26.89612	-0.1336633	-0.31711
1997/8	28.76561	1.7358239	1.89183	2001/9	26.58893	-0.4408588	-0.44843
1997/9	28.8835	1.85371413	2.039827	2001/10	26.65296	-0.3768203	-0.55593
1997/10	29.11574	2.08595211	2.13381	2001/11	26.50218	-0.5276056	-0.59421
1997/11	29.2096	2.17981429	2.092827	2001/12	26.26643	-0.7633588	-0.44617
1997/12	29.16545	2.13566365	1.949702	2002/1	26.53811	-0.4916761	-0.09505
1998/1	28.99279	1.96300339	1.768084	2002/2	26.94631	-0.083471	0.365429
1998/2	28.78022	1.75043929	1.62178	2002/3	27.31978	0.28999057	0.7781
1998/3	28.62059	1.59080788	1.450466	2002/4	27.91955	0.88976621	1.133692
1998/4	28.55388	1.52409314	0.884387	2002/5	28.18433	1.15454185	1.15443
1998/5	28.26628	1.23649698	0.113463	2002/6	28.38655	1.35676942	1.01491
1998/6	26.92236	-0.1074293	-0.72537	2002/7	27.98176	0.95197775	0.82935
1998/7	26.24111	-0.7886793	-1.10129	2002/8	27.76577	0.73598416	0.838431
1998/8	25.74979	-1.2799934	-1.34133	2002/9	27.82987	0.80008673	0.992485
1998/9	25.79458	-1.2352017	-1.45165	2002/10	28.00901	0.97922134	1.066951
1998/10	25.52099	-1.5087915	-1.73582	2002/11	28.22793	1.19814762	0.987977
1998/11	25.41883	-1.6109549	-1.87428	2002/12	28.05327	1.02348416	0.770995
1998/12	24.94207	-2.0877178	-1.80833	2003/1	27.77208	0.74229827	0.692416
1999/1	25.10563	-1.9241601	-1.32878	2003/2	27.57699	0.54720211	0.715381
1999/2	25.61667	-1.4131184	-0.71543	2003/3	27.81753	0.78774698	0.672501
1999/3	26.38074	-0.6490479	-0.24368	2003/4	27.84098	0.8111925	0.567122
1999/4	26.94566	-0.084128	-0.02662	2003/5	27.44835	0.41856429	0.434221
1999/5	27.03192	0.00213801	-0.22025	2003/6	27.50139	0.47160916	0.268719
1999/6	27.03192	0.00213801	-0.66886	2003/7	27.44228	0.41249057	0.10608
1999/7	26.36476	-0.6650254	-1.09391	2003/8	26.95184	-0.0779421	0.040712
1999/8	25.68611	-1.3436793	-1.31654	2003/9	27.01348	-0.0163075	0.095696
1999/9	25.75676	-1.2730222	-1.46398	2003/10	27.24617	0.2163848	0.081273
1999/10	25.69686	-1.3329261	-1.72786	2003/11	27.11679	0.0870098	-0.04438
1999/11	25.2438	-1.785987	-2.0143	2003/12	26.97021	-0.0595767	-0.09729
1999/12	24.96511	-2.0646729	-1.98016	2004/1	26.8692	-0.1605864	-0.03303
2000/1	24.83753	-2.192253	-1.60246	2004/2	26.95808	-0.0717081	0.294723
2000/2	25.34623	-1.6835511	-0.86874	2004/3	27.163	0.13321173	0.66357
2000/3	26.09822	-0.9315639	-0.26678	2004/4	27.85245	0.82266686	0.875129
2000/4	27.03869	0.00890083	0.050092	2004/5	28.06462	1.03483032	0.81116
2000/5	27.1521	0.12231429	-0.04547	2004/6	27.79768	0.76789121	0.632277
2000/6	27.04885	0.01906108	-0.27786	2004/7	27.66054	0.6307598	0.535354
2000/7	26.75199	-0.2777979	-0.54528	2004/8	27.52796	0.49817968	0.465263
2000/8	26.45495	-0.5748331	-0.78711	2004/9	27.50691	0.47712198	0.534569
2000/9	26.24657	-0.7832146	-0.97175	2004/10	27.45027	0.42048737	0.487346
2000/10	26.02649	-1.0032947	-1.13941	2004/11	27.73588	0.70609634	0.402645
2000/11	25.90106	-1.1287274	-1.17627	2004/12	27.36524	0.33545532	0.18896
2000/12	25.74357	-1.2862113	-1.07247	2005/1	27.19617	0.1663848	0.253121
2001/1	25.91591	-1.1138716	-0.6828	2005/2	27.09482	0.06503865	0.547832
2001/2	26.21247	-0.8173171	-0.13705	2005/3	27.55772	0.52793929	0.910701
2001/3	26.91256	-0.117221	0.336385	2005/4	28.0803	1.05051942	1.07147
2001/4	27.55317	0.52338801	0.582384	2005/5	28.18343	1.15364442	0.875151
2001/5	27.63277	0.60298737	0.494275	2005/6	28.04003	1.01024698	0.465194

2005/7	27.49135	0.46156109	0.026871	2009/8	27.48893	0.45914121	0.500044
2005/8	26.95356	-0.0762274	-0.20317	2009/9	27.33215	0.30236237	0.702202
2005/9	26.72506	-0.304721	-0.37417	2009/10	27.76841	0.73862839	0.969558
2005/10	26.80122	-0.2285671	-0.62065	2009/11	28.0954	1.06561557	1.012373
2005/11	26.44056	-0.5892242	-0.95079	2009/12	28.13421	1.10442968	0.951059
2005/12	25.98564	-1.044144	-1.03372	2010/1	27.89686	0.86707391	0.959189
2006/1	25.81079	-1.2189998	-0.79376	2010/2	27.91146	0.88167327	1.061075
2006/2	26.19176	-0.8380222	-0.20197	2010/3	28.15861	1.1288207	0.908821
2006/3	26.70551	-0.3242722	0.37404	2010/4	28.20252	1.17273096	0.483815
2006/4	27.58617	0.5563848	0.749894	2010/5	27.4547	0.42491044	-0.23864
2006/5	27.91979	0.8900066	0.677047	2010/6	26.88359	-0.1461953	-0.89005
2006/6	27.83308	0.80329186	0.449889	2010/7	26.03514	-0.9946408	-1.45289
2006/7	27.36763	0.33784314	0.291716	2010/8	25.50048	-1.5293043	-1.80657
2006/8	27.23832	0.20853224	0.3456	2010/9	25.19505	-1.834737	-1.97246
2006/9	27.35856	0.32877262	0.523735	2010/10	24.97412	-2.0556665	-2.12487
2006/10	27.52928	0.49949378	0.660183	2010/11	25.00282	-2.0269646	-2.14016
2006/11	27.77272	0.74293929	0.465557	2010/12	24.73782	-2.2919646	-1.95949
2006/12	27.7679	0.73811557	0.112955	2011/1	24.92822	-2.1015639	-1.46882
2007/1	26.9454	-0.0843844	-0.10497	2011/2	25.54486	-1.4849293	-0.76621
2007/2	26.71492	-0.3148652	0.126363	2011/3	26.20982	-0.8199614	-0.18379
2007/3	27.11413	0.08434955	0.372902	2011/4	27.03606	0.00627262	0.158703
2007/4	27.63939	0.60960596	0.457475	2011/5	27.29212	0.26233032	0.065749
2007/5	27.45454	0.42475019	0.15186	2011/6	27.23729	0.2075066	-0.3521
2007/6	27.36785	0.3380675	-0.29698	2011/7	26.7572	-0.2725896	-0.81233
2007/7	26.72255	-0.307237	-0.91573	2011/8	26.03856	-0.9912274	-1.16124
2007/8	26.10801	-0.9217722	-1.4029	2011/9	25.8566	-1.1731825	-1.37162
2007/9	25.5116	-1.5181825	-1.75101	2011/10	25.71046	-1.3193203	-1.51253
2007/10	25.26103	-1.7687594	-1.93464	2011/11	25.40744	-1.6223492	-1.60966
2007/11	25.06369	-1.9660992	-2.06356	2011/12	25.43386	-1.5959229	-1.37919
2007/12	24.96072	-2.0690639	-2.06266	2012/1	25.41907	-1.6107146	-0.97386
2008/1	24.87428	-2.1555062	-1.67889	2012/2	26.09885	-0.9309389	-0.31205
2008/2	25.06638	-1.9634069	-1.01381	2012/3	26.64986	-0.3799293	0.180584
2008/3	26.11202	-0.9177658	-0.32652	2012/4	27.4045	0.37471814	0.561513
2008/4	26.86952	-0.1602658	0.003335	2012/5	27.57675	0.54696173	0.600573
2008/5	27.12825	0.09846814	0.069665	2012/6	27.79264	0.76285916	0.547293
2008/6	27.10159	0.07180147	-0.05869	2012/7	27.52168	0.49189762	0.286951
2008/7	27.06851	0.03872455	-0.30324	2012/8	27.41691	0.38712198	0.07553
2008/8	26.74319	-0.286596	-0.55227	2012/9	27.01162	-0.0181665	-0.16057
2008/9	26.36795	-0.6618364	-0.73827	2012/10	26.88742	-0.1423652	-0.32325
2008/10	26.32141	-0.7083748	-0.98622	2012/11	26.70861	-0.3211793	-0.56902
2008/11	26.18518	-0.8446088	-1.21883	2012/12	26.52359	-0.5061953	-0.67321
2008/12	25.6241	-1.4056825	-1.25263	2013/1	26.15011	-0.8796729	-0.46578
2009/1	25.62359	-1.4061953	-0.8356	2013/2	26.39603	-0.6337594	0.025108
2009/2	26.08378	-0.946003	-0.19259	2013/3	27.14588	0.11609634	0.401609
2009/3	26.87519	-0.1545928	0.417523	2013/4	27.62277	0.59298737	0.437357
2009/4	27.55261	0.52282711	0.822736	2013/5	27.52553	0.49574378	0.173981
2009/5	27.91412	0.88433352	0.87491	2013/6	27.25313	0.22333993	-0.18265
2009/6	28.09083	1.06104827	0.73318	2013/7	26.83264	-0.1971408	-0.40363
2009/7	27.70913	0.67934955	0.480284	2013/8	26.45563	-0.5741601	-0.54164

2013/9	26.59021	-0.4395767	-0.48082	2017/10	26.32466	-0.7051216	-1.04519
2013/10	26.41861	-0.6111793	-0.50101	2017/11	25.90753	-1.122253	-1.22017
2013/11	26.63808	-0.3917081	-0.57763	2017/12	25.7216	-1.3081825	-1.12956
2013/12	26.52963	-0.5001537	-0.68045	2018/1	25.79971	-1.2300735	-0.8346
2014/1	26.18877	-0.841019	-0.51796	2018/2	26.17938	-0.8504101	-0.33085
2014/2	26.32962	-0.7001697	0.007662	2018/3	26.60646	-0.4233267	0.192282
2014/3	27.0171	-0.0126857	0.611882	2018/4	27.31096	0.28117647	0.6103
2014/4	27.76563	0.73583993	0.875551	2018/5	27.74878	0.71899698	0.670877
2014/5	28.14228	1.11249057	0.685113	2018/6	27.86051	0.83072775	0.42615
2014/6	27.80811	0.77832391	0.305445	2018/7	27.49269	0.46290724	0.144745
2014/7	27.19431	0.16452583	0.028783	2018/8	27.0146	-0.0151857	0.130888
2014/8	27.00327	-0.0265158	0.002074	2018/9	27.0163	-0.013487	0.288132
2014/9	26.97813	-0.0516601	0.131412	2018/10	27.45112	0.42133673	0.410728
2014/10	27.11418	0.08439762	0.201876	2018/11	27.48633	0.45654506	0.285984
2014/11	27.39128	0.36149698	0.137913	2018/12	27.38409	0.35430147	0.251924
2014/12	27.18952	0.15973416	0.083495	2019/1	27.07689	0.04710596	0.251946
2015/1	26.92229	-0.1074934	0.284483	2019/2	27.38415	0.35436557	0.726508
2015/2	27.22803	0.19824378	0.83334	2019/3	27.38415	0.35436557	1.12483
2015/3	27.79248	0.76269891	1.357715	2019/4	28.50058	1.47079186	1.384627
2015/4	28.56886	1.53907711	1.680263	2019/5	28.57912	1.54933352	1.103863
2015/5	28.80115	1.77136878	1.740242	2019/6	28.16354	1.1337566	0.497352
2015/6	28.76013	1.73034314	1.710103	2019/7	27.65829	0.62850019	0.004221
2015/7	28.7488	1.71901301	1.738319	2019/8	26.75958	-0.2702017	-0.13511
2015/8	28.71074	1.68095211	1.880407	2019/9	26.68415	-0.3456344	0.017816
2015/9	28.84478	1.81499057	2.142133	2019/10	27.2403	0.21051942	0.117645
2015/10	29.17506	2.14527903	2.24068	2019/11	27.21835	0.18856429	0.062758
2015/11	29.49591	2.46612839	2.166096	2019/12	26.98364	-0.0461472	0.007197
2015/12	29.14042	2.1106316	1.926112	2020/1	27.07564	0.04585596	0.219547
2016/1	28.95131	1.92152903	1.798094	2020/2	27.05167	0.0218816	0.601983
2016/2	28.77596	1.74617647	1.757384	2020/3	27.62069	0.59090403	0.788447
2016/3	28.75636	1.72657711	1.581492	2020/4	28.22295	1.19316365	0.675781
2016/4	28.82918	1.79939762	1.199414	2020/5	27.61106	0.58127262	0.2817
2016/5	28.24829	1.21850019	0.557662	2020/6	27.28269	0.25290724	-0.1438
2016/6	27.61013	0.58034314	-0.0916	2020/7	27.04071	0.01092006	-0.63901
2016/7	26.90393	-0.1258588	-0.57274	2020/8	26.33455	-0.6952338	-1.17582
2016/8	26.3005	-0.7292883	-0.86289	2020/9	25.79707	-1.2327178	-1.48872
2016/9	26.16671	-0.8630703	-0.86152	2020/10	25.43029	-1.5994966	-1.58982
2016/10	26.03348	-0.9963075	-0.81883	2020/11	25.39583	-1.6339517	-1.5152
2016/11	26.30462	-0.7251697	-0.74787	2020/12	25.49377	-1.536019	-1.30228
2016/12	26.29476	-0.7350255	-0.56211	2021/1	25.65417	-1.3756184	-0.88546
2017/1	26.24638	-0.7834069	-0.16989	2021/2	26.03458	-0.9952017	-0.33977
2017/2	26.86188	-0.1679101	0.509558	2021/3	26.74423	-0.2855543	0.122678
2017/3	27.47143	0.44164121	0.991134	2021/4	27.29122	0.26143288	0.405888
2017/4	28.28473	1.2549425	1.20607	2021/5	27.42194	0.39215403	0.285835
2017/5	28.3066	1.2768175	0.97521	2021/6	27.59386	0.56407711	-0.03243
2017/6	28.11623	1.08644891	0.455728	2021/7	26.93106	-0.0987274	-0.48643
2017/7	27.59215	0.56236237	-0.11614	2021/8	26.46715	-0.5626376	-0.85953
2017/8	26.74816	-0.281628	-0.53863	2021/9	26.23188	-0.7979101	-1.0981
2017/9	26.40064	-0.629144	-0.81884	2021/10	25.81175	-1.2180383	-1.30194

2021/11	25.75143	-1.2783588	-1.32989
2021/12	25.62037	-1.4094165	-1.27741
2022/1	25.72788	-1.3019005	-1.12918
2022/2	25.90888	-1.1209069	-0.84037
2022/3	26.06505	-0.964737	-0.58878
2022/4	26.59433	-0.4354581	-0.3273
2022/5	26.66364	-0.3661472	-0.37552
2022/6	26.8495	-0.1802819	-0.65154
2022/7	26.44966	-0.5801216	-1.06565
2022/8	25.83558	-1.1942081	-1.33036
2022/9	25.60718	-1.4226056	-1.37402
2022/10	25.65551	-1.3742722	-1.35241
2022/11	25.7046	-1.3251857	-1.3146
2022/12	25.672	-1.3577819	-1.14472
2023/1	25.76894	-1.2608428	-0.63196
2023/2	26.21426	-0.8155222	0.099942
2023/3	27.21026	0.18047134	0.785819
2023/4	27.96466	0.93487839	1.189467
2023/5	28.27189	1.24210596	1.247795
2023/6	28.4212	1.39141686	1.204387
2023/7	28.13965	1.10986237	1.110872
2023/8	28.14167	1.1118816	1.141273
2023/9	-	-	1.364069
2023/10	28.20045	1.17066365	1.429558
2023/11	28.58726	1.55747455	1.560535

The Oceanic Niño Index (ONI) serves as the principal metric used by NOAA to track the oceanic aspect of the El Niño-Southern Oscillation (ENSO) climate phenomenon. It concentrates on the east-central tropical Pacific Ocean, spanning from 120° to 170°W longitude and from 5°N to 5°S latitude near the International Dateline. This designated area is known as the Niño-3.4 region, recognized as pivotal for monitoring sea surface temperature (SST) variations associated with ENSO. Determining the intensity of El Niño-Southern Oscillation (ENSO) events is a key focus for researchers due to its significant impacts on society, ecology, and the economy. These intensities are known to undergo decadal variations. conducted a study utilizing the envelope function of Sea Surface Temperature (SST) in the Niño 3.4 and Niño 3 regions during boreal winter to identify a 10–15-year modulation cycle in ENSO intensity. They established criteria based on the 3-month average Sea Surface Temperature Anomaly (SSTA) in the Niño 3.4 area to categorize ENSO intensity. Events with SSTA values ranging from 0.5 to 0.9 are classified as weak, 1.0 to 1.4 as moderate, 1.5 to 1.9 as strong, and

above 2.0 as very strong. These classifications were applied to characterize El Niño and La Niña events spanning from 1950 to 2021.

According to the values calculated by the Oceanic Niño Index, the years 1987-1988, 1997-98 and 2015-16 are observed to be very strong EL-Niño years. During this period the values of the ONI for certain months are observed to be more than +2.0. The highest value of ONI was observed for the month of October 1997 is +2.133 and for October 2015 at +2.166092. However, the highest value for the 1987 super El-Niño is 1.755258. The years 1999-2000, 2007-2008 and 2010-2011 are observed to be very strong La-Niña years the highest value of ONI for 1999-2000 is -2.0143 in 1999. The next highest value of ONI was observed in 2007 which is -2.06266. The highest value of ONI out of all 3 very strong La-Niñas was observed during the La-Niña of 2010-2011 which is -2.14016. The year 2023 is also observed to be a strong El Niño year the highest ONI value observed during November 2023 is +1.560535.

4.4 Precipitation Over Indian Ocean

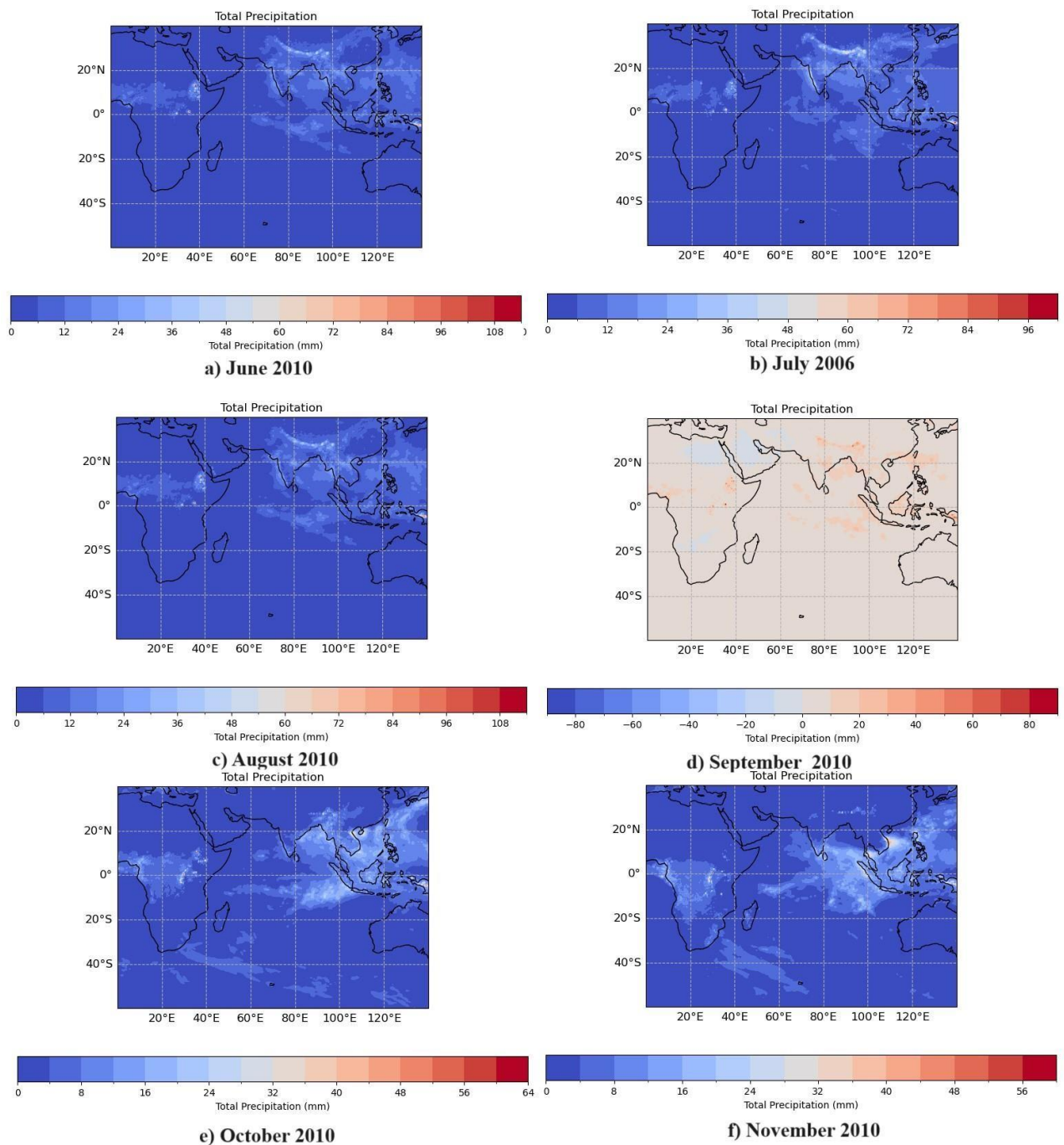


Fig 4.4.1 Precipitation over the Indian Ocean in the year 2010 a strong La- Nina year.

Figure 4.4.1 shows the total precipitation over India and Indian Oceans. The El Niño-Southern Oscillation (ENSO) significantly influences precipitation patterns over India and the Indian Ocean. During El Niño events, warm oceanic waters lead to altered atmospheric circulation patterns, causing a weakening of the Indian summer monsoon. This weakening results in decreased rainfall over large

parts of India, particularly in the central and southern regions. Conversely, during La Niña events, cooler ocean temperatures lead to enhanced monsoon circulation, resulting in above-average rainfall in many parts of the country. The impacts of ENSO on Indian precipitation can have far-reaching consequences, affecting agricultural productivity, water resources, and socio-economic conditions. Timely forecasts of ENSO events are crucial for anticipating and managing these impacts, helping to mitigate risks and enhance resilience in vulnerable communities across India. The plot covers over 0-140 E and 40-60 S. The maximum rainfall observed is 0 mm and the maximum temperature observed is 66mm. Sea surface precipitation up to 34mm is denoted by blue contours and precipitation beyond 34 mm is denoted by red contours.

Figure 4.4.1 is a series of total precipitation over the Indian Ocean region from June 2010 to November 2010. India experiences monsoon during June, July, and August and post-monsoon during September, October, and November. The year 2010 experienced a strong La-Nina phase due to which we observed around 40-50mm of rainfall over the western Ghat region. In June 2010 the major part of the Bay of Bengal, the coastal region around the Bay of Bengal, and the coast of India around the Arabian sea received rainfall of about 40-50mm. parts of Indonesia received rainfall of around 20-30mm. parts of Africa also received around 40-50 mm of rainfall. During July high amount of rainfall was observed over the central and northeastern parts of India few regions received rainfall of more than 60mm. Also, parts of Africa received more than 50 mm of rainfall. In the month of August, a slight decrease in precipitation was observed over the northeastern parts but the African region received a similar amount of rainfall as observed in the month of July. During the post-monsoon season, only the northeastern and the parts of south India are observed to have received about significant amount of rainfall. During September only the Northeast part of India is observed to receive precipitation about 30-40mm. However, in parts of Africa, the rate of precipitation is observed to be increased. The precipitation is observed to further decrease in October in the northeastern parts of India but the precipitation over the central part of Africa is further observed to increase. In the month of November, no Precipitation is observed over the Northeastern parts of India. Central parts and Southern parts of Africa receive 20-30mm of rainfall. Precipitation is observed to increase in

Parts of Indonesia, Myanmar, and southern parts of China. During the months of June, July, and August the western ghat region and the central region receive precipitation of about 30-40 mm, and certain regions like northeastern parts of India and eastern parts of Africa receive precipitation of about 40-60mm. During the months of September, October, and November the central and southern parts of Africa, Southern parts of India, and parts of Myanmar, Indonesia, and southern parts of China receive 20-30mm of rainfall and other parts receive less or no precipitation.

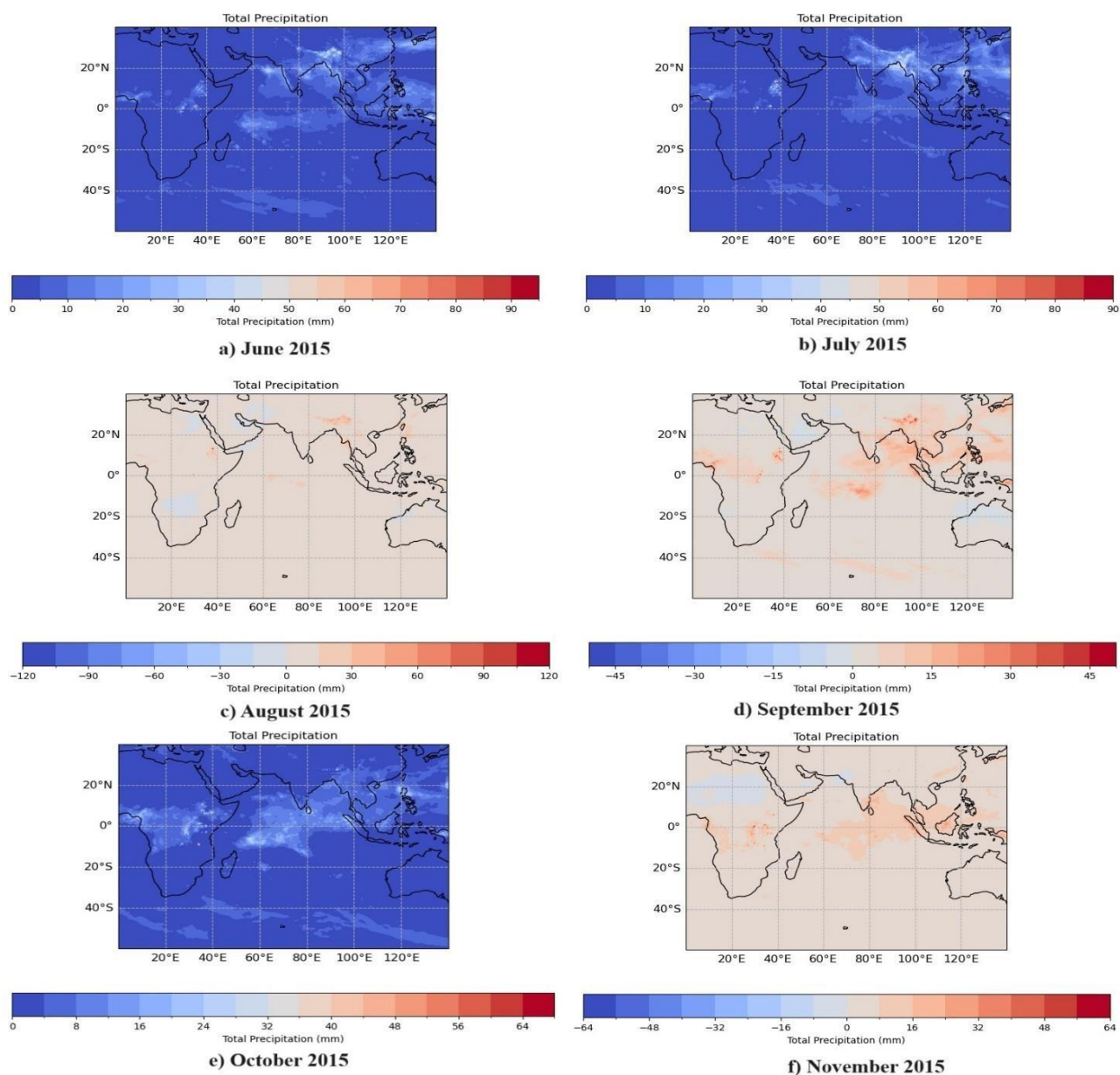


Fig 4.4.2 Precipitation over the Indian Ocean in the year 2015 a super strong El-Nino year.

Fig 4.8 is a series of total precipitation over the Indian Ocean region from June 2015 to November 2015. India experiences monsoon during June, July, and August and post-monsoon during September,

October, and November. The year 2015 experienced a strong El-Nino phase due to which we observed around 30-40mm of rainfall over the western Ghat region. Also July high amount of rainfall was observed over the central and northeastern parts of India during July. During the post-monsoon season, only the northeastern and the parts of south India are observed to have high amounts of rainfall. During the El-Nino phase, the precipitation observed is comparatively lesser than that observed during the La Nina phase. In June 2015 the major part of the Bay of Bengal, the coastal region around the Bay of Bengal, and the coast of India around the Arabian Sea received rainfall of about 30-40mm. Parts of Indonesia received rainfall around 20-30mm. Parts of Africa and northeastern parts of India receive around 40-50 mm of rainfall. During July high amount of rainfall was observed over the central and northeastern parts of India few regions received rainfall of more than 60mm. Also, parts of Africa received more than 50 mm of rainfall. However, western ghats are observed to receive lesser rainfall compared to the month of June. In the month of August on only the northeastern parts of India and parts of Ethiopia receive rainfall anywhere between 30-60mm and the rest of the regions are observed to have absolutely low or No rainfall. During the post-monsoon season, only the northeastern and the parts of India are observed to have received about significant amount of rainfall. During September only the Northeast part of India is observed to receive precipitation of about 30-40mm. However in central and southern parts of Africa, Indonesia the rate of precipitation is observed to be increased. Around 15-30 mm of rainfall is observed over these regions. In the month of October, the central parts of Africa and central parts of the Indian Ocean receive 20-30mm of rainfall. In the month of November no Precipitation is observed over the North eastern parts of India. Central parts and Southern part of Africa receives 20-30mm of rainfall. Precipitation is observed to increase Parts of Indonesia, Myanmar and southern parts of China. Generally, during the months of June, July, and August the western ghat region and the central region receive precipitation of about 30-40 mm, and certain regions like north eastern parts of India and eastern parts of Africa receive precipitation of about 40-60mm but this trend is not observed during 2015 monsoon season. very low or no precipitation was observed over the western Ghats and the central parts of India. During the months of September, October, and November the central and

southern parts of Africa , Southern parts of India and parts of Myanmar, Indonesia and southern parts of China receive 20-30mm of rainfall and other parts receive less or no precipitation. A higher amount of precipitation was observed during the La-Nina phase than the El-Nino phase.

4.5 Discussion

4.5.1 Sea Surface Temperature

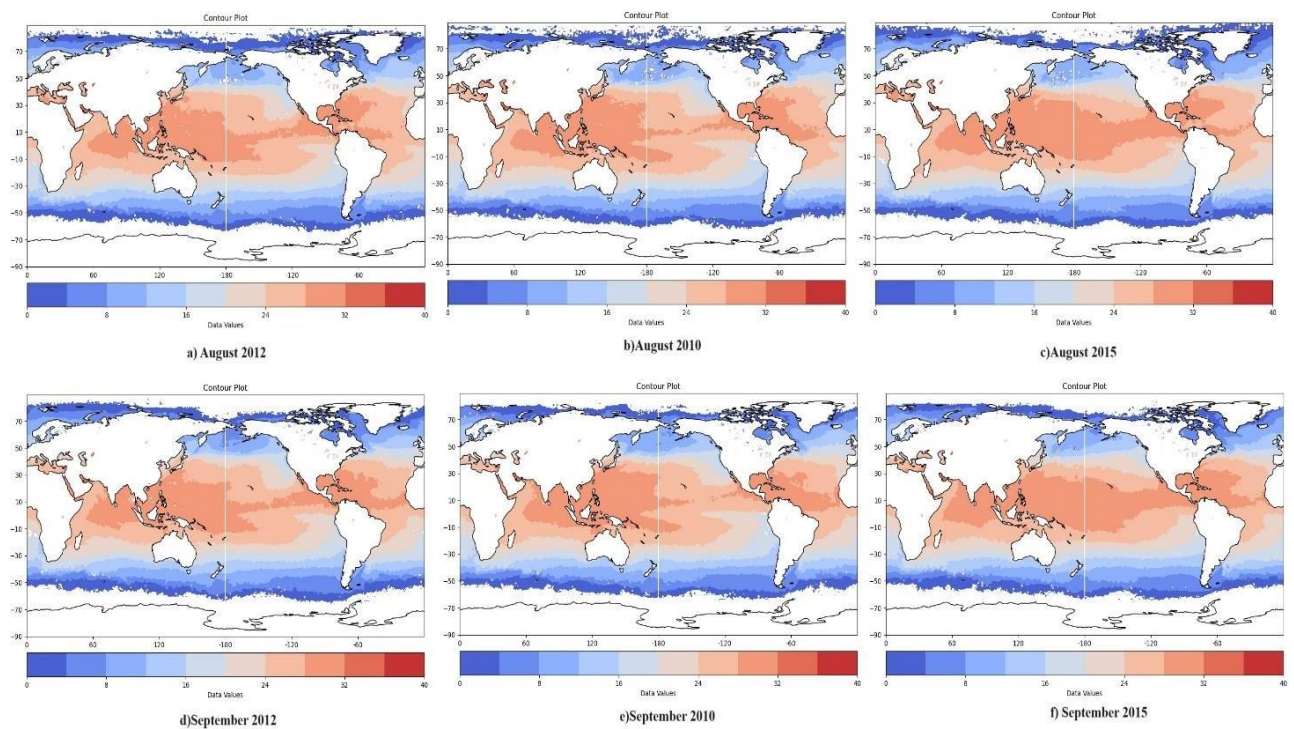


Figure 4.5.1 Monthly Mean Of Sea Surface Temperature over a) August 2012 b) August 2010 c) August 2015 d) September 2012 e) September 2012 f) October 2012

Fig 4.5.1 is a plot of SST over the global region for August 2012 the SST near the central and Eastern Pacific Ocean is observed to be around 24° C. The year 2012 was observed to be a neutral phase where no El-Nino or La-Nina existed . Fig b) is a plot of SST over the global region for August 2010. The temperature is observed to be around 24 ° C. The year 2010 experienced a Super strong La-Nina Fig c) is a plot of SST over the global region for August 2015. Where the temperature near the central and eastern Pacific Ocean is observed to be around 28° C. The year 2015 experienced a Super strong El Nino. fig d) is a plot of SST over the global region for September 2012 the SST near the central and Eastern Pacific Ocean is observed to be slightly increased as the northern hemisphere experiences boreal summer from June to August. e) plot of SST over the global region for September 2010 the SST.

According to NCEP Generally, the SST is often observed to peak during September as the northern hemisphere experiences boreal summer from June to August but this trend was not observed during

September 2010 (<https://www.cpc.ncep.noaa.gov>). f) plot of SST over the global region for September 2015 the SST. During this year the sea surface temperature is observed to be much higher than normal or as compared to that in September 2012. According to **McPhaden et al. (2006)**, “During an El Niño year, weakening winds along the equator lead to warming water surface temperatures that lead to further weakening of the winds.” During the El Niño-Southern Oscillation (ENSO), sea surface temperature (SST) anomalies in the tropical Pacific Ocean influence the strength and frequency of El Niño events. Warmer-than-average SSTs in the central and eastern Pacific characterize El Niño phases, weakening trade winds and altering atmospheric circulation patterns. This leads to widespread climatic impacts, including shifts in rainfall patterns, droughts, and floods globally. These fluctuations disrupt ecosystems, agriculture, and economies, underscoring the pivotal role of SST in driving ENSO dynamics. The variations in sea surface temperatures (SST) observed during different years, particularly in the central and eastern Pacific Ocean, are primarily driven by the El Niño-Southern Oscillation (ENSO) phenomenon. ENSO refers to the cyclical variation in SST and atmospheric conditions across the tropical Pacific Ocean, encompassing El Niño and La Niña events, as well as neutral phases.

During a La Niña event, cool surface waters accumulate in the central and eastern Pacific, leading to cooler-than-average SST. This was evident in August 2010, when the super strong La Niña event resulted in SST around 24° C. Conversely, during an El Niño event, warmer surface waters spread across the central and eastern Pacific, causing warmer-than-average SST, as seen in August 2015 with SST reaching approximately 28° C during a super strong El Niño event.

In contrast, neutral phases occur when neither El Niño nor La Niña conditions dominate, resulting in relatively stable SST, as observed in August 2012 with SST around 24° C. However, even during neutral phases, other climate patterns and regional influences can affect SST, leading to slight variations. The transition from August to September can also influence SST. Typically, during the northern hemisphere's boreal summer from June to August, SST tends to peak. This was evident in September 2012, when SST slightly increased compared to August due to seasonal warming.

However, in September 2010, SST didn't follow the expected trend, indicating the influence of other climatic factors that may have suppressed the typical warming. (<https://earthobservatory.nasa.gov>.)

4.5.2 Sea Surface Temperature Anomaly

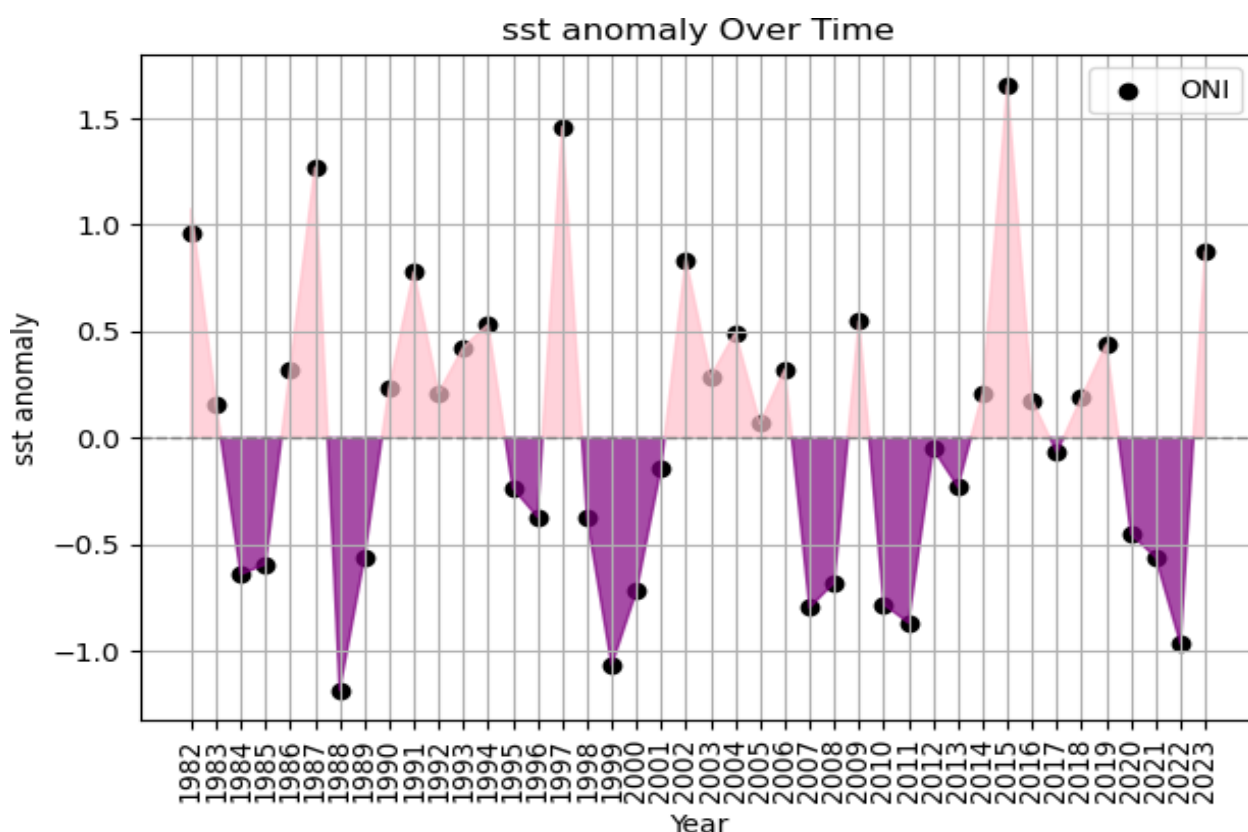


Fig 4.5.2 variation of SSTA over last 40 years over the Nino 3.4 region.

Fig 4.5.2 is a plot of SSTA over 40 years. Where the positive SSTA values are denoted in pink color and the negative values are denoted in purple. The highest positive values are observed in the years 1982, 1987, 1997 and 2015. The lowest values are observed over 1988, 1999, 2011 and 2022.

The observed patterns in temperature variations across different phases of the El Niño-Southern Oscillation (ENSO) phenomenon can be attributed to the complex interactions between oceanic and atmospheric conditions in the tropical Pacific region.

During El Niño events, warmer-than-average sea surface temperature anomalies are typically observed in the central and eastern Pacific Ocean, particularly around the longitude -170° . This

warming is associated with a weakening of the trade winds and a reduction in the upwelling of cold water from the ocean depths. As the intensity of El Niño increases, the warming effect becomes more pronounced, leading to higher temperatures in this region.

Conversely, during La Niña events, cooler-than-average sea surface temperatures prevail in the central and eastern Pacific Ocean. The temperature around longitude -120° tends to decrease during La Niña phases, especially as the intensity of La Niña increases. This cooling effect is often attributed to stronger trade winds and enhanced upwelling of cold water from the ocean depths. The reduced temperature uniformity during the La Niña phases may result from these intensified regional cooling effects.

Very high sea surface temperature (SST) anomaly values can occur due to a combination of factors including strong El Niño events, long-term climate change trends leading to global warming, localized ocean heat waves, specific environmental conditions such as reduced cloud cover and decreased wind speeds, geographical features like shallow coastal waters and ocean currents, oceanographic events disrupting normal circulation patterns, and extreme weather phenomena such as hurricanes or prolonged periods of high insolation. These factors interact in complex ways to amplify SST anomalies, resulting in elevated ocean temperatures that can have significant impacts on marine ecosystems, weather patterns, and global climate dynamics.

Low sea surface temperature (SST) values can be attributed to various natural and anthropogenic factors. La Niña events, characterized by cool ocean currents in the equatorial Pacific, often result in reduced SST values as cooler-than-average waters prevail in the central and eastern Pacific Ocean. Additionally, upwelling phenomena, driven by wind patterns and ocean currents, can bring cold, nutrient-rich water from deeper layers to the surface, leading to localized cooling along coastal regions. While long-term global warming trends generally elevate SST values, localized cooling can occur due to changes in atmospheric circulation patterns or the influence of cold ocean currents and geographical features. Extreme weather events such as storms or periods of cloud cover can disrupt normal heating processes, resulting in temporary cooling of SST values.

Moreover, natural variability in ocean temperatures, influenced by seasonal changes, ocean

circulation, and atmospheric dynamics, can contribute to fluctuations in SST, occasionally leading to periods of lower-than-average temperatures. These factors collectively underscore the complex interplay of natural processes and human-induced influences shaping ocean temperatures and SST anomalies.

4.5.3 Oceanic Niño Index

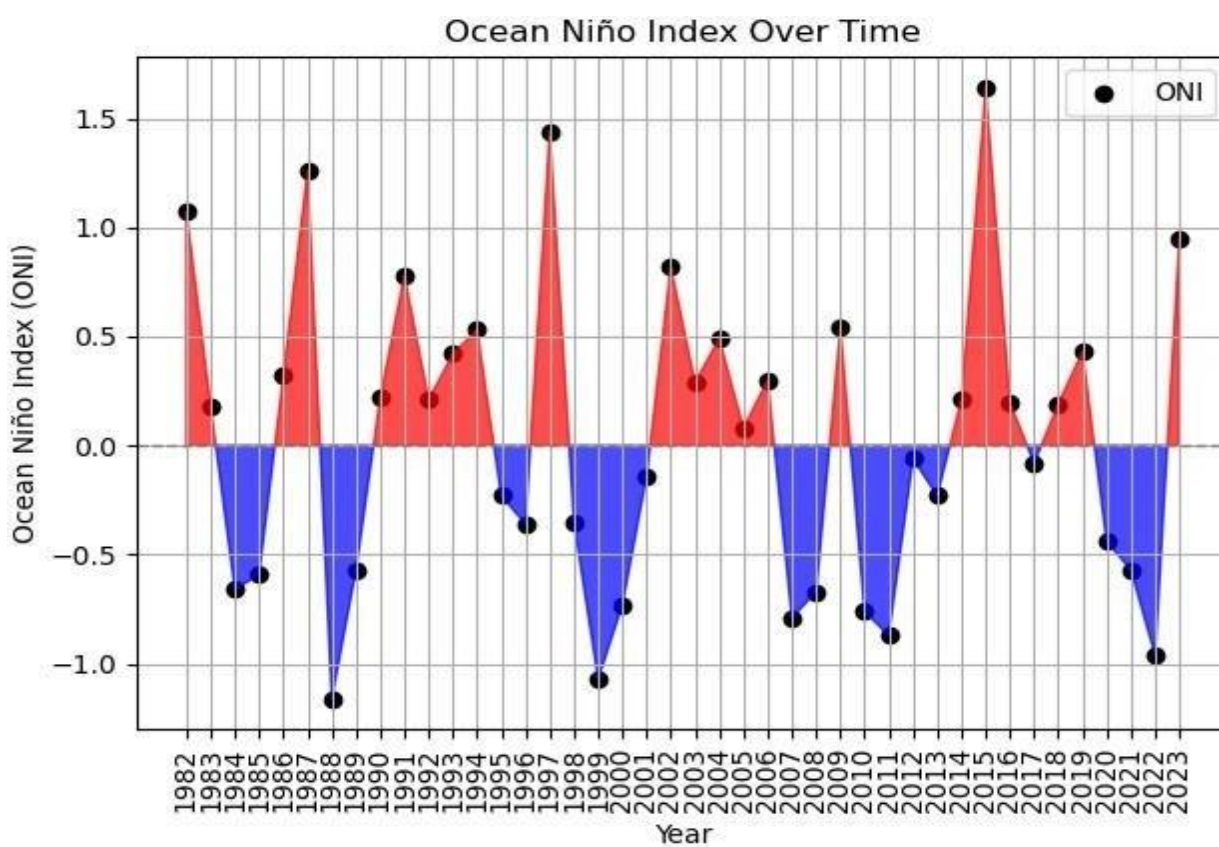


Fig 4.5.3 variation of ONI over last 40 years over the Niño 3.4 region.

Fig 4.5.3 represents is an Oceanic Niño Index Plot for the last 40 years the events are categorized as Weak if the ONI values is between 0.5 and 0.9°C, Moderate if the ONI values are between 1.0 and 1.4°C, Strong if the ONI values are between 1.5 and 1.9°C, or Very Strong if the ONI values $\geq 2.0^\circ\text{C}$ based on the extent and duration of the anomaly. This classification system ensures a standardized approach to understanding and predicting these significant climate phenomena.

According to the Oceanic Nino Index plot, the years 1987-1988,1997-98 and 2015-16 are observed to be very strong EL-Nino years. During this period the values of the ONI for certain months are observed to be more than +2.0. The highest value of ONI was observed for the mean of 1997 is +2.133 and for 2015 at +2.166092. However, the highest value for the 1987 super El-NINO is 1.755258. The strong Elnino years are mostly followed by the La-nina years. The years 1999-2000,2007-2008 and 2010-2011 are observed to be very strong La-Nina years the highest value of ONI for 1999-2000 is -2.0143 in 1999. The next highest value of ONI was observed in 2007 which is -2.06266. The highest value of ONI out of all 3 very strong La-Ninas was observed during the La-Nina of 2010-2011 which is -2.14016. The year 2023 is also observed to be a strong El Nino year the highest ONI value observed during November 2023 is +1.560535.

Table 4.5.1 El-Nino phases observed over the last 40 years.

Weak El-Nino	Moderate El-Nino	Strong El-Nino	Very Strong El-Nino
2004-2005	1987	1982-1983	1987-1988
	2009-2010	1991-1992	1997-1998
			2015-2016

Table 4.5.2 La-Nina Phases observed over the last 40 years.

Weak La-Nina	Moderate La-Nina	Strong La-Nina	Very strong La-Nina
1983-1984	1995-1996	1988-89	1999-2000
2005-2006	2011-2012	1998-99	2007-2008
2016-2017			2010-2011

4.5.4 Precipitation Over Indian Ocean

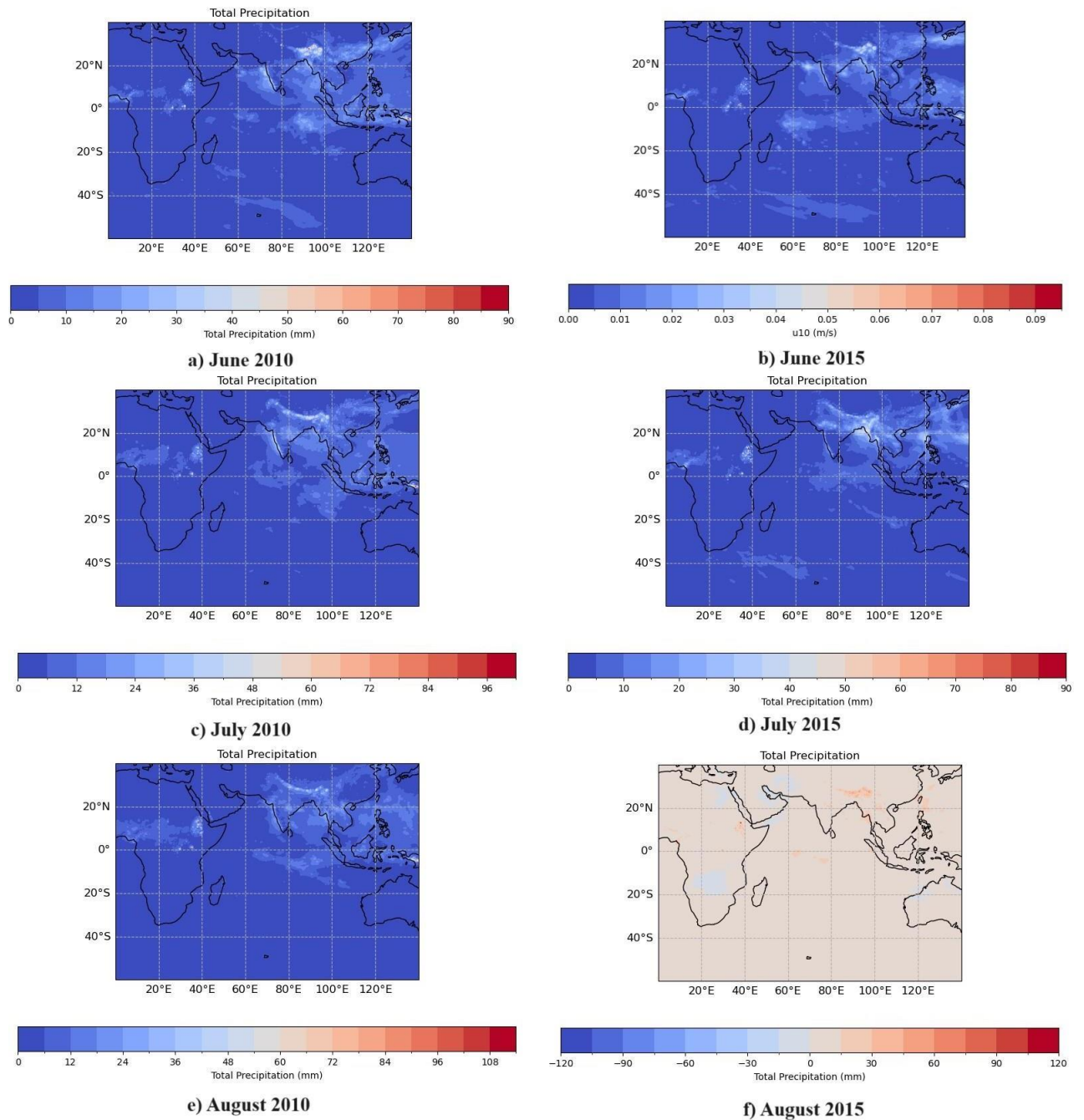


Fig 4.5.4 Total precipitation over the Indian Ocean region from June to August 2010 and 2015. Figure 4.5.4 shows total precipitation over the Indian Ocean In June 2010 the major part of the Bay of Bengal, the coastal region around the Bay of Bengal, and the coast of India around the Arabian Sea received rainfall of about 40-50mm. Parts of Indonesia received rainfall of around 20-30mm. parts of Africa also receive around 40-50 mm of rainfall. During July high amount of rainfall was observed over the central and northeastern parts of India few regions received rainfall of more than

60mm. Also, parts of Africa received more than 50 mm of rainfall. In August slight decrease in precipitation was observed over the northeastern parts but the African region received a similar amount of rainfall as observed in July. In June 2015 the major part of the Bay of Bengal, the coastal region around the Bay of Bengal, and the coast of India around the Arabian Sea received rainfall of about 30-40mm. Parts of Indonesia received rainfall around 20-30mm. Parts of Africa and northeastern parts of India receive around 40-50 mm of rainfall. During July high amount of rainfall was observed over the central and northeastern parts of India few regions received rainfall of more than 60mm. Also, parts of Africa received more than 50 mm of rainfall. However western ghats are observed to receive lesser rainfall compared to June. In August only the northeast parts of India and parts of Ethiopia receive rainfall anywhere between 30-60mm and the rest of the regions are observed to have low or No rainfall. A higher amount of precipitation was observed during the La-Nina phase than the El-Nino phase. A large variation of rainfall was seen over the western ghats and central parts of India. The western Ghat region and central India receive more rainfall during the La-Nina phase and the El-Nino phase.

During El Niño years, India experienced drier conditions in the southern regions, leading to reduced agricultural productivity and water shortages, while the northern parts may see slightly warmer temperatures and erratic rainfall patterns. In Africa, Eastern countries like Ethiopia and Kenya face heavy rainfall and flooding, affecting crops and displacing populations, whereas Southern African nations like Zimbabwe and South Africa endure drought conditions, impacting agriculture and water resources. Indonesia witnesses drier-than-average conditions, particularly in regions like Sumatra and Kalimantan, leading to forest fires and haze, which have significant environmental and economic consequences. Conversely, during La Niña years, India sees increased rainfall in the south and along the west coast, potentially causing flooding, while the north experiences cooler temperatures. Eastern Africa receives above-average rainfall, leading to floods, while Southern Africa finds relief from drought conditions, aiding agricultural productivity. Indonesia experiences increased rainfall, reducing drought and forest fire risk, but increasing the potential for flooding and landslides. These climatic variations significantly impact agriculture, water resources, and livelihoods across India,

Africa, and Indonesia, underscoring the importance of understanding and monitoring El Niño and La Niña events for effective climate risk management.

During the strong El Niño event of 2015-2016, southern India experienced severe drought conditions. Tamil Nadu, for instance, faced a water crisis with reservoirs drying up and agricultural losses amounting to billions of rupees. In 1997-1998, Eastern Africa experienced severe flooding attributed to El Niño. Kenya suffered from widespread flooding, leading to displacement of populations, destruction of homes, and loss of lives. The El Niño event of 2015 resulted in extensive forest fires and haze in Indonesia. The haze blanketed parts of Sumatra and Kalimantan, causing air quality to plummet, health issues to rise, and economic losses due to disruptions in tourism and agriculture.

In contrast, the La Niña event of 2010-2011 brought heavy rainfall to parts of southern India. Kerala witnessed devastating floods, with thousands displaced and significant damage to infrastructure and crops. During the La Niña event of 2007-2008, Southern Africa faced a severe drought, particularly affecting countries like Zimbabwe. This led to widespread crop failure, food shortages, and economic distress. The La Niña event of 2010 brought relief to drought-stricken regions of Indonesia. Increased rainfall helped replenish water sources, reduce the risk of forest fires, and support agricultural activities.

4.6 Conclusion

The analysis presented highlights the intricate interplay between oceanic and atmospheric conditions, particularly during different phases of the El Niño-Southern Oscillation (ENSO) phenomenon. Through the examination of sea surface temperature (SST) anomalies, Oceanic Niño Index (ONI) plots, and precipitation patterns over specific regions, a comprehensive understanding of the climatic impacts of El Niño and La Niña events emerges.

Sea surface temperature (SST) is a critical indicator of climate variability and plays a pivotal role in driving global climate patterns. SST refers to the temperature of the ocean's surface layer, which is influenced by various factors including solar radiation, air-sea interactions, ocean currents, and atmospheric circulation patterns. Changes in SST can have profound impacts on marine ecosystems, weather patterns, and global climate dynamics.

During El Niño events, warmer-than-average SST anomalies are typically observed in the central and eastern Pacific Ocean, particularly along the equatorial region. This warming is attributed to a weakening of the trade winds and a reduction in the upwelling of cold water from the ocean depths. As the intensity of El Niño increases, the warming effect becomes more pronounced, leading to higher SST values in affected regions. Conversely, during La Niña events, cooler-than-average SST prevails in the central and eastern Pacific Ocean due to stronger trade winds and enhanced upwelling of cold water from deeper ocean layers.

SST anomalies (SSTA) provide a measure of deviation from the long-term average SST values for a particular period. Positive SSTA indicates warmer-than-average SST, while negative SSTA indicates cooler-than-average SST. These anomalies are crucial for identifying the presence and intensity of El Niño and La Niña events, as they reflect the magnitude of temperature anomalies in key regions of the tropical Pacific Ocean. Positive SSTA values during El Niño events signify the presence of anomalously warm waters, while negative SSTA values during La Niña events indicate anomalously cool waters.

The Oceanic Niño Index (ONI) is a standardized measure used to categorize and quantify the strength of El Niño and La Niña events based on SST anomalies in the equatorial Pacific Ocean. ONI values are calculated by averaging SST anomalies over specific regions and periods. The ONI classification system categorizes events as weak, moderate, strong, or very strong based on the extent and duration of the anomaly. For example, ONI values between 0.5°C and 0.9°C denote weak El Niño or La Niña, while values $\geq 2.0^{\circ}\text{C}$ indicate very strong events.

Understanding SST, SSTA, and ONI is essential for monitoring and predicting ENSO events and their associated climatic impacts. These metrics serve as key indicators for assessing the likelihood and severity of El Niño and La Niña events, enabling decision-makers to implement appropriate mitigation and adaptation strategies. Moreover, SST anomalies provide valuable insights into the underlying ocean-atmosphere interactions driving ENSO dynamics, facilitating ongoing research and modeling efforts aimed at improving our understanding of climate variability and change.

In summary, SST, SSTA, and ONI are integral components of the broader climate system, offering valuable information about the state of the tropical Pacific Ocean and its influence on global climate patterns. By monitoring these indicators, scientists and policymakers can enhance their ability to anticipate and respond to the impacts of El Niño and La Niña events, ultimately contributing to more effective climate risk management and adaptation efforts worldwide.

REFERENCES

Books and papers

- Bader, J., & Latif, M. (2003). The impact of decadal-scale Indian Ocean Sea surface temperature anomalies on Sahelian rainfall and the North Atlantic Oscillation. *Geophysical Research Letters*, 30(22).
- Belliard, J. P., Dominguez-Granda, L. E., Ramos-Veliz, J. A., Rosado-Moncayo, A. M., Nath, J., Govers, G., ... & Temmerman, S. (2021). El Niño driven extreme sea levels in an Eastern Pacific tropical river delta: Landward amplification and shift from oceanic to fluvial forcing. *Global and Planetary Change*, 203, 103529.
- Builes-Jaramillo, A., Valencia, J., & Salas, H. D. (2023). The influence of the El Niño-Southern Oscillation phase transitions over the northern South America hydroclimate. *Atmospheric Research*, 290, 106786.
- Cane, M. A. (2005). The evolution of El Niño, past and future. *Earth and Planetary Science Letters*, 230(3-4), 227-240.
- Chen, D., & Cane, M. A. (2008). El Niño prediction and predictability. *Journal of Computational Physics*, 227(7), 3625-3640.
- Choi, H. M., Kim, M. K., & Yang, H. (2023). Deep-learning model for sea surface temperature prediction near the Korean Peninsula. *Deep Sea Research Part II: Topical Studies in Oceanography*, 208, 105262.
- Derot, J., Sugiura, N., Kim, S., & Kouketsu, S. (2024). Improved climate time series forecasts by machine learning and statistical models coupled with signature method: A case study with El Niño. *Ecological Informatics*, 79, 102437.
- Emile-Geay, J., Cane, M., Seager, R., Kaplan, A., & Almasi, P. (2007). El Niño as a mediator of the solar influence on climate. *Paleoceanography*, 22(3).

- Glantz, M. H., & Ramirez, I. J. (2020). Reviewing the Oceanic Niño Index (ONI) to enhance societal readiness for El Niño's impacts. *International Journal of Disaster Risk Science*, *11*, 394-403.
- Hafez, Y. (2016). Study on the relationship between the oceanic nino index and surface air temperature and precipitation rate over the Kingdom of Saudi Arabia. *Journal of Geoscience and Environment Protection*, *4*(05), 146.
- Harrison, D. E., & Larkin, N. K. (1998). El Niño-Southern Oscillation Sea surface temperature and wind anomalies, 1946–1993. *Reviews of Geophysics*, *36*(3), 353-399.
- Jia, L., He, Y., Liu, W., Zhang, Y., & Li, Y. (2022). Assessment of drought events in Southwest China in 2009/2010 using sun-induced chlorophyll fluorescence. *Forests*, *14*(1), 49.
- Liyanage, P., Tozan, Y., Tissera, H. A., Overgaard, H. J., & Rocklöv, J. (2022). Assessing the associations between Aedes larval indices and dengue risk in Kalutara district, Sri Lanka: a hierarchical time series analysis from 2010 to 2019. *Parasites & Vectors*, *15*(1), 277.
- McPhaden, M. J., Zebiak, S. E., & Glantz, M. H. (2006). ENSO as an integrating concept in earth science. *science*, *314*(5806), 1740-1745.
- Philander, S. G. (1999). El Nino and La Nina predictable climate fluctuations. *Reports on Progress in Physics*, *62*(2), 123.
- Ren, H. L., Zuo, J., & Deng, Y. (2019). Statistical predictability of Niño indices for two types of ENSO. *Climate Dynamics*, *52*, 5361-5382.
- Stewart, R. H. (2008). *Introduction to physical oceanography*. Robert H. Stewart.
- Trenberth, K. E., Caron, J. M., Stepaniak, D. P., & Worley, S. (2002). Evolution of El Niño–Southern Oscillation and global atmospheric surface temperatures. *Journal of Geophysical Research: Atmospheres*, *107*(D8), AAC-5.
- Tudhope, A. W., Chilcott, C. P., McCulloch, M. T., Cook, E. R., Chappell, J., Ellam, R. M., ... & Shimmield, G. B. (2001). Variability in the El Niño-Southern Oscillation through a glacial-interglacial cycle. *Science*, *291*(5508), 1511-1517.

- Wang, G. G., Cheng, H., Zhang, Y., & Yu, H. (2023). ENSO analysis and prediction using deep learning: A review. *Neurocomputing*, 520, 216-229.
- Wang, S., Mu, L., & Liu, D. (2021). A hybrid approach for El Niño prediction based on Empirical Mode Decomposition and convolutional LSTM Encoder-Decoder. *Computers & Geosciences*, 149, 104695.
- Wolter, K., & Timlin, M. S. (2011). El Niño/Southern Oscillation behaviour since 1871 as diagnosed in an extended multivariate ENSO index (MEI. ext). *International Journal of Climatology*, 31(7), 1074-1087.
- Zhou, Q., & Wei, L. (2023). Influence of the pace of El Niño decay on tropical cyclone frequency over the western north pacific during decaying El Niño summers. *Atmospheric and Oceanic Science Letters*, 16(3), 100328.

Websites

- <http://www.bom.gov.au/climate/about/australian-climate-influences>
- <https://www.climate.gov/news-features/understanding-climate>
- <https://neo.gsfc.nasa.gov>
- <https://earthobservatory.nasa.gov>